Combining graphene with silicon carbide: synthesis and properties - a review

Ivan Shtepliuk, Volodymyr Khranovskyy and Rositsa Yakimova

Journal Article

Original Publication:

Ivan Shtepliuk, Volodymyr Khranovskyy and Rositsa Yakimova, Combining graphene with silicon carbide: synthesis and properties - a review, Semiconductor Science and Technology, 2016. 31(11), pp.113004.
http://dx.doi.org/10.1088/0268-1242/31/11/113004

Combining graphene with silicon carbide: synthesis and properties – a review

Ivan Shtepliuk, Volodymyr Khranovskyy and Rositsa Yakimova

Department of Physics, Chemistry and Biology, Linköping University, SE-58183, Linköping, Sweden

Corresponding author: Rositsa Yakimova, e-mail: rosya@ifm.liu.se

Abstract

Being a true two-dimensional crystal, graphene possesses a lot of exotic properties that would enable unique applications. Integration of graphene with inorganic semiconductors, e.g. SiC promotes the birth of a class of hybrid materials which are highly promising for development of novel operations, since they combine the best properties of two counterparts in the frame of one hybrid platform. As a specific heterostructure, graphene on SiC performs strongly dependent on the synthesis method and the growth modes.

In this paper a comprehensive review of the most relevant studies of graphene growth methods and mechanisms on SiC substrates has been carried out. The aim is to elucidate the basic physical processes that are responsible for the formation of graphene on SiC.

First, an introduction is made covering some intriguing and not so often discussed properties of graphene. Then, we focus on integration of graphene with SiC which is facilitated by the nature of SiC to assume graphitization. As concerning the synthesis methods we discuss thermal decomposition of SiC, chemical vapor deposition and molecular beam epitaxy stressing that the first technique is the most common one when SiC substrates are used. In addition, we briefly appraise graphene synthesis via metal mediated carbon segregation.

We address in detail the main aspects of the substrate effect such as substrate face polarity, off-cut, kind of polytype and nonpolar surfaces on the growth of graphene layers. A comparison of graphene grown on the polar faces is made. In particular, growth of graphene on Si-face SiC is critically analyzed concerning growth kinetics and growth mechanisms taking into account the specific characteristics of SiC (0001) surfaces, such as the step-terrace structure and the unavoidable surface reconstruction upon heating. In all subtopics obstacles and solutions are featured. We complete the review with a short summary and concluding remarks.

Outline

1. Introduction to graphene

The ever-growing development of technologies, an increase in life dynamics and needs of mankind in improving ecological and economical situations bring enormous demands for discoveries of new physical and chemical phenomena, design and fabrication of multifunctional materials and manufacturing of next-generation electronic devices. The 20th century was an unprecedented historical period, full of great scientific discoveries (including those in the field of quantum physics, semiconductor physics and solid state physics), which marked the beginning of a new digital nano-world, appearance of the unique high-precision experimental methods for material characterization and significant update of the theoretical physics. It has definitely allowed the scientists to make a qualitative leap forward in solving many of the existing problems, for example, the realization of *p*-type conductivity in gallium nitride, the discovery of new nanomaterials, silicon electronics miniaturization, gradual improvement of the efficiency of solar cells and light-emitting diodes, *etc*. Alone among these achievements is a renewed interest in carbon and its allotropes having intriguing properties depending on the dimension and offering a plethora of practical applications [1].

The historical path of carbon began with the use and study of its three-dimensional (3D) forms (diamond, graphite), continued by discovery of zero-dimensional (0D) fullerenes [2] and one-dimensional (1D) nanotubes [3], and currently extends into investigations of its two-dimensional (2D) allotrope, *graphene*. Recently, a new stable honeycomb carbon allotrope (or three-dimensional graphene) was also synthesized by deposition of vacuum-sublimated graphite [4].

For the first time the term «*graphene*» was used in 1962 by H. P. Boehm et al. [5] who reported on extremely thin carbon films obtained by reduction of graphite oxide. Further progress in the synthesis and study of this material was associated primarily with improving the techniques for its identification, an accurate determination of the thickness and the measurement of electronic properties. From a scientific and technological point of view, such

a development dynamics could be expected, since although being a building block of buckyballs, nanotubes and graphite, graphene has long been considered as an unattainable material due to natural reasons. In particular, it was mistakenly believed that graphene is a thermodynamically unstable material, because a strict long-range order in the atomic arrangement in the two-dimensional case could not be realized at the finite temperatures [6, 7]. In other words, it was suggested impossible to synthesize a true two-dimensional crystal, i.e. a crystal with a strictly planar periodic arrangement of particles (atoms or molecules).While the band structure of graphene was theoretically predicted by Wallace [8] in 1947 and Slonczewski et al. [9] in 1958, it took more than half a century before Kostya Novoselov and Andre Geim were able to realize the ghost-material in 2004 [10]. A surprise is not even the huge time interval between the prediction and discovery of graphene, but the simplicity of the synthesis technology with a conventional adhesive tape. Graphene field started to explode in 2004, being accompanied by simultaneous improvement of its quality, development of experimental methods for its fabrication and identification, demonstration of new physics effects and more recently the creation of graphene-based hybrid structures. The Nobel Prize in Physics 2010 was deservedly awarded to the graphene pioneers. Although it is important to acknowledge the contributions of other research groups into the development of this area of physics, whose work determined the occurrence of a variety of methods for the synthesis of graphene (molecular beam epitaxy, MOCVD, high-temperature sublimation, intercalation) and created the conditions for the implementation of its exotic properties. In particular, the initial evidences of graphene were firstly reported a few decades ago by Morgan et al. [11], May [12], Shelton *et al.* [13] and Van Bommel *et al.* [14]. Furthermore, almost simultaneously with the publication of Geim and Novoselov, Berger *et al.* [15] have proposed a method for the synthesis of the so-called epitaxial graphene on silicon carbide substrates that has predetermined further developments of this material and proved the possibility of its real use in various electronic devices.

What makes graphene so unique? What are its intriguing properties, causing the huge interest of researchers and the rapid development? Answers to these questions can be found in the detailed understanding of its crystal structure, chemical bonds and energy band spectrum using complementary chemical, crystallographic and physical approaches. Let us begin to explain briefly the difference between an isolated carbon atom and graphene. From a chemical point of view, four unpaired electrons are present on the outer shell of a carbon atom and can participate in the formation of chemical bonds. When graphene is composed in a honeycomb lattice sheet, three of the four electrons form strong covalent bonds with neighboring atoms in

the lattice due to the overlap of sp^2-hybridized orbitals (the bonding energy is estimated to be 5.9 eV). The fourth electron not involved in the formation of chemical bonds is in $2p_z$ state and participates in the electrical conductivity. Such π electrons are above and below the planar structure. Robustness and strength of the covalent carbon-carbon bond make graphene the strongest material in the world with mechanical stiffness as high as 1 TPa [16]. In addition, the strong and anisotropic in-plane bonding as well as unique phonon properties of graphene (existence of flexural lattice vibrational phonon modes) are responsible for the record-high thermal conductivity ~$5 \cdot 10^3$ $W \cdot m^{-1} \cdot K^{-1}$[17, 18].

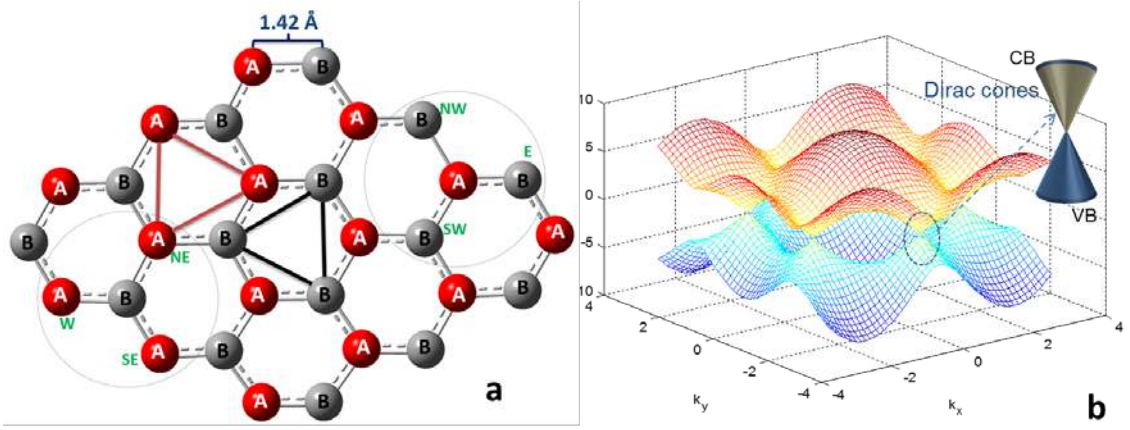

Figure 1. (a) Honeycomb lattice of graphene with consideration of two different triangular carbon sublattices (red and black), (b) energy band structure of graphene, which was calculated in Matlab using the well-known Wallace formalism.

Graphene has a unique crystal structure, which can be represented by two equivalent carbon sublattices *A* and *B* (see Figure 1a). It is due to the fact that the honeycomb lattice is not Bravais lattice in the conventional meaning of this term often used in crystallography. According to the generally accepted definition, the term Bravais lattice implies that all lattice sites must be equivalent, while any vectors connecting the lattice sites must be primitive lattice vectors. Nevertheless, these conditions are not satisfied in the case of the honeycomb lattice of graphene, because of two neighboring carbon atoms are not equivalent by default. In particular, carbon atom belonging to *A* sublattice has three nearest neighbors in the three directions: north-west (NW), south-west (SW), and east (E). While each carbon atom in *B* sublattice forms the sp^2 bonds with three carbon atoms in the north-east (NE), west (W), and south-east (SE) directions (Figure 1a). Therefore, the hexagonal lattice of graphene cannot be ascribed to Bravais lattice, but each of sublattices is a primitive triangular Bravais lattice. It should be noted

that the distance between two nearest carbon atoms is only 1.42 Å. As an important consequence of such a unique crystal structure, the movement of the charge carriers within graphene obeys Dirac-like formalism rather than the conventional Schrödinger equation. Due to this the hopping between *A* and *B* sublattices causes the formation of two cosine-like energy bands intersecting at zero energy near the edges of the Brillouin zone. As a result of this intersection of energy bands, two cone-like parts (touching each other near the Dirac points K and K′) of the energy spectrum at the absolute value of energy not exceeding 1eV occur (Fig. 1b). Aforementioned features lead to two important consequences. First, in contrast to the conventional semiconductors, where electrons obey a parabolic-like energy dispersion and have an effective mass, the free carriers in graphene follow a linear dispersion relation and behave as massless relativistic quasi-particles with unprecedented high mobility of ~100 000 $cm^2 \cdot V^{-1} \cdot s^{-1}$ and Fermi velocity of ~$1.10 \cdot 10^6$ m/s. Second, the two-dimensional honeycomb lattice of graphene displays a sublattice (chiral) symmetry [19]. It should be mentioned that chiral symmetry proper to graphene is responsible for direct observation of some of transport phenomena in graphene, for example, so-called Klein paradox. Generally, the Klein paradox in graphene can be understood as tunneling of quasiparticles (Dirac fermions) through a high and wide potential barrier [20].

Aforementioned structural and chemical features define not only the unique band structure of graphene (absence of energy gap, the formation of the Dirac cones at *K* and *K´* points of the Brillouin zone, the possibility of engineering the Fermi level and the density of states with the help of external influence), but also the unusual peculiarities of carriers (lack of effective electron mass, high Fermi velocity, huge mobility, "V"-shaped conductivity with respect to charge density *n*), and intriguing properties in the presence of magnetic field (Shubnikov–de Haas oscillations for the longitudinal conductivity σ_{xx} and unusual quantum Hall plateaux for the Hall conductivity σ_{xy} at a sufficiently strong magnetic field). It should be mentioned that the anomalous integer quantum Hall effect in graphene is associated with the appearance of the electronic Landau levels near the Dirac point in the magnetic field [21].

Moreover, the strong interaction of graphene with light in a wide wavelength range (from far-infrared to visible) makes this material promising for use in optoelectronics, plasmonics and photonics, because of the possibility of excitation of interband and intraband transitions, the generation of surface plasmons and hybrid plasmon-polaritons. Broadly speaking, the optical properties of graphene are almost entirely governed by the peculiarities of its band structure. In particular, the processes of light absorption and optical conductivity in the terahertz range and the far infrared region are determined mainly by intraband transitions (the

so-called intraband free-carrier absorption). In this range the properties of graphene are similar to those of noble metals and may be described by Drude theory. With increasing energy to $2E_F$ (E_F –Fermi energy), the absorption by free carriers is reduced and, as a result of the Pauli restrictions for interband transitions, optical conductivity in the mid-infrared region reaches its minimum value. Further increase in energy leads to that optical conductivity in the near infrared and visible region is completely determined by interband transitions and reaches its universal value. The absorption in this region is 2.3%. Moreover many-body effects at energies above 3 eV lead to the appearance of a singularity with a maximum of 4.6 eV, associated with the exciton resonance in the M point of the Brillouin zone. Since the position of the Fermi level in graphene (as opposed to metal) can be controlled, it opens up more opportunities for the implementation of engineering the optical and electronic properties. In fact, graphene is a plasmonic material [22]. But since the processes of light absorption in the near infrared and visible spectral range are accompanied by mostly generation of electron-hole pairs (the transition from the valence band into the conduction band), the excitation of surface plasmons with energies greater than $2E_F$ is impossible because of the Landau damping mechanism. Therefore, the existence of graphene plasmons is limited only by terahertz and far-infrared regions on conditions that the plasmon dispersion curve does not intersect with a continuum of intraband transitions. Fig. 2 summarizes most important properties of graphene.

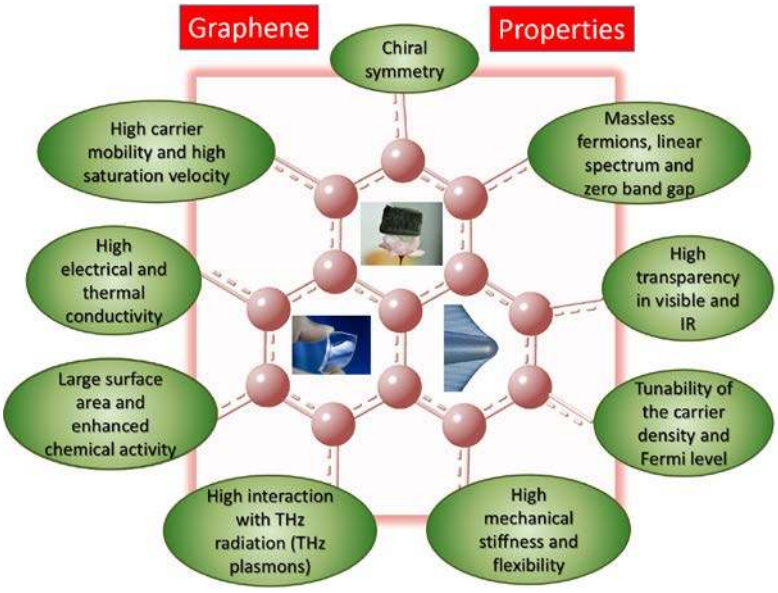

Figure 2. Summary of the most important properties of graphene.

Most of the unique properties of graphene can be observed and manifest themselves only when the monoatomic layer does not interact with the growth interface and insulating substrates using for transferring the graphene films. Failure to comply with these conditions

can lead to the appearance of an energy gap, additional doping, occurrence of a buffer layer that chemically interacts with the substrate, increasing the carrier concentration and a decrease in carrier mobility. Therefore, methods for synthesis of graphene should promote obtaining a homogeneous monoatomic layer whose atoms do not take part in the formation of chemical bonds with the atoms of the substrate. Moreover, the use of graphene in electronics requires implementation of its growth technology on large area insulating substrates. The most common fabrication methods of graphene can be classified into four groups by synthesis's principles, where each of them has its own advantages and disadvantages.

i. The first group includes mechanical exfoliation of highly oriented pyrolytic graphite using adhesive tape, followed by clamping the tape to the substrate of silicon dioxide and transfer of the shelled graphene onto its surface [10, 23]. In fact, this method is non-productive, because it is difficult to obtain a uniform film thickness over a large area (lateral dimensions of films on substrates are typically of the order of up to tens of micrometers) [24]. This method, in spite of its technological shortcomings, allows to obtain high-quality crystals of graphene with extremely high value of carrier mobility. For example, the value of carrier mobility as high as 120 000 $cm^2 \cdot V^{-1} \cdot s^{-1}$ has been measured at temperature of 240 K by Bolotin et al. [25].

ii. The second group comprises graphene synthesis using chemical methods [26] including the reduction of a single-layer graphite oxide film, manipulations with carboxyl groups of graphene and using polymer matrices. The quality of the graphene obtained in this manner is much lower in comparison to graphene obtained by mechanical exfoliation, due to the incomplete removal of various functional groups and a difficult control of complex chemical reactions.

iii. The third group includes methods that use an external carbon source for a direct growth of graphene films (chemical vapor deposition and molecular beam epitaxy). The advantages of these methods are (i) the possibility of growth on large-area dielectric and conductive substrates, (ii) low growth temperature, promoting technological benefits. However, the need to control the quality of the substrate, the purity of the external carbon source, and the need of transfer in most cases reduce the use of these methods to limited applications.

iv. The last, fourth group consists of methods based on thermal decomposition (Si sublimation) of a silicon carbide (SiC) substrate and is the most operative. This is primarily due to the convenience of the synthesis and the ability to manipulate graphene quality by controlling face polarity, off-cut angle, kind of polytype and

eventually the type of intercalant. From an experimental point of view, the epitaxial graphene films grown by sublimation on semi-insulating SiC substrates are the most suitable objects for study by optical and electrical methods and for device fabrication.

Concerning graphene growth, a lot of excellent review papers has been published earlier, for example [27-32]. In the present review paper we describe some important aspects of the growth mechanisms of graphene on Si-face SiC substrates that can be important for the graphene quality. Although growth of graphene on carbon-face (C-face) is of great interest we do not focus on it here in detail. Readers can easily find experimental details regarding the growth features of graphene involving the carbon-face SiC in several relevant reports [33-39]. We provide only brief description of the differences between some properties of graphene on C-face and Si-face SiC. We believe that the growth technology based on thermal decomposition of silicon-face SiC is more suitable and attractive for practical applications due to the possibility to achieve large-scale uniform graphene layers. Thus, this approach deserves more scrupulous and careful attention. Nevertheless, it is fair to note that the absence of the buffer layer in the case of graphene on C-face SiC is promoting higher values of the carrier mobility in comparison to that of graphene on Si-face SiC [36].

Seemingly, the research of pristine, "simply" graphene is already passing its zenith and the next stage in the development of graphene is its utilization in hybrid structures and devices with other materials and, especially, with such having an energy band gap. There are several brilliant review articles discussing the advantages of the so called Van der Waals heterostructures formed between graphene and other 2D materials [40] and we do not focus on that subject here. According to the Web of Science database within the period from 1985 to 2016 a total of 63 330 documents devoted to graphene has been published. Figure 3a shows the interest time evolution of the scientific community in the study of graphene, indicating an exponential growth of the publication numbers with time. Analysis of the papers published in 2014-2016 indicates that the main efforts of scientists at the present time has shifted from the study of the fundamental properties of graphene to their implementation in creating biosensors, removal of hazardous substances, development of photocatalysts, supercapacitors and ion batteries (Fig. 3b).

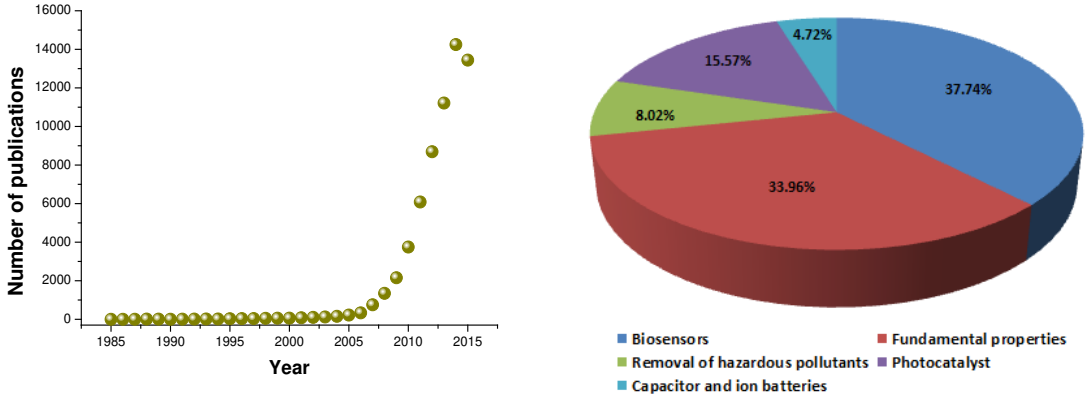

Figure 3. (a) Time evolution of the number of publications according to Web of science database and (b) Percentage of the worldwide publications in 2016 by graphene' research area.

This review paper is organized as follows. Section 1 describes the historical path of graphene from an unrealizable concept to the Nobel Prize material and gives a sound explanation of the unprecedented scientific hype. Section 2 provides background in graphene growth by thermal decomposition of silicon carbide. In this section, we review the state-of-the-art of graphene growth with consideration of different effects emerging from the integration of graphene with SiC. In Sections 2, the recent progress in the growth of graphene on SiC by using the external carbon sources and metal mediators is also reviewed. Section 3 presents our concluding remarks.

2. Integration of graphene with SiC

2.1. Graphene by thermal decomposition of SiC

Thermal decomposition of Si-face silicon carbide substrates to achieve graphene growth has emerged in the last decade from a laboratory method that deals with unmanageable graphene uniformity and thickness, to a reproducible technology of growing large-scale, uniform epitaxial graphene layers with the desired thickness that can be further implemented to design various electronic devices. Such a remarkable transition has been facilitated by two important factors.

- First, the effect of SiC substrates on the physical properties of the graphene layers has been successfully established. In fact, a correct assessment and clear understanding of the substrate's role are highly important for choosing the most appropriate applications of epitaxial graphene. It opens up a possibility of graphene growth *directly* on insulting substrates. That is strongly beneficial for simplification of processing technology of field effect transistors, avoiding

complicated multi-stage technological procedure of graphene transfer to foreign dielectric substrates.

- Second, new technological approaches of controlling graphene growth and novel applications to use epitaxial layers have both been proposed.

Unlike graphene layers on C-face SiC possessing high rotational disorder producing Moiré patterns, graphene on Si-face surfaces has only one rotational orientation with respect to the substrate [41]. An important point is that the surface energy of the C-face (718 erg/cm^2) is smaller than that of Si-face (1767 erg/cm^2) [21, 42]. Small surface energy can initiate an uncontrolled Si sublimation rate and induce the formation of inhomogeneities in the graphene layers [43]. For these reasons, high structural quality monolayer (1ML) graphene films on Si-face can be grown over large areas, whereas the reproducible and scalable growth on C-face (that could, in principle, lead to better electronic properties) is still elusive. However, despite the technological attractiveness the growth of graphene on Si-face has its own bottleneck and disadvantages. In particular, the graphene growth is accompanied by the formation of graphene-like C-rich buffer layer with $\left(6\sqrt{3}\times 6\sqrt{3}\right)R30^{\circ}$ surface reconstruction [44]. A distinctive feature of this interface layer is its interaction with the substrate. About 30% of the carbon atoms forming the reconstructed surface are bound to the Si atoms of the topmost layer of SiC substrate, resulting in charge transfer between graphene and the substrate as well as in degradation of graphene electronic properties via sp^3 hybridization - electron doping and substrate-related carrier scattering mechanisms being involved. Thus, it is a great challenge to obtain buffer-free epitaxial graphene films demonstrating exceptional two-dimensional properties. The main strategy to activate the non-conductive graphene-like buffer layer is the recovery of the destroyed π bands by breaking the strong covalent bonding to the SiC substrate. Decoupling the buffer layer and further restoring of the π-bands and enhancement of the conductivity has been successfully achieved [45] by using non-metallic (O[46], H [47],Si [48], Ge[49],water vapour [50], F[51]) and metallic intercalants (Al [52], Li[53], Pt [54], Au[55], Na[56], Yb[57], Fe[58], Ca [59], Cs [60], Cu[61]). Intercalant species are able to diffuse towards the interface between the buffer layer and the Si-face SiC substrate and to create bonds with the topmost Si atoms, thereby leading to the conversion of the buffer layer to a quasi-free-standing graphene. Noteworthy is that the attempts to intercalate C-face graphene have not been successful.

2.1.1. Brief comparison of graphene grown on C-face and Si-face SiC

Commonly, the commercial wafers of SiC are cut perpendicularly to the *c*-axis of the grown crystal. Because of the polar nature of the two faces, respectively Si-terminated (0001) face and C-terminated (000-1) face of a silicon carbide wafer, the polarity of SiC significantly influences the structural and chemical features of the surface and interface for growth of graphene. It has been shown that the quality of epitaxial graphene can be varied by the polarity, as shown in Table 1. It can be explained by the fact that both, the rearrangement of the C-C bonds in the honeycomb planar structure and the formation of defects are related to the growth mechanism, which in turn depends on the polarity of the surface. Strictly speaking, the growth mechanisms of graphene layers on Si-face and C-face SiC substrates are governed by similar physical processes that are related to high-temperature sublimation of Si atoms due to the difference in the vapor pressures of silicon and carbon. While Si is sublimating, the remaining carbon atoms undergo self-organization in the graphene structure with strong in-plane sp^2 bonds. In spite of the similarity of the underlying physical processes for both faces, there is an observable inequality in surface reconstructions and growth kinetics for each polar surface. These factors are responsible for different etching rate, surface diffusion, growth kinetics and interface morphologies. Consequently, the electronic, optical and morphological properties of the graphene layers, which are formed on SiC substrates exhibiting different crystallographic polarities, can differ from each other. In this context it is of crucial importance to understand the mechanisms of graphene formation depending on the crystallographic polarity. In this Section we review some graphene growth features related to the crystal polarity of SiC in different stacking sequences (polytypes).

Strong evidences of face-dependent surface reconstruction of SiC during graphene growth have been reported by Emtsev *et al.* [35]. Probably the first theoretical report on the SiC face polarity effect on the single layer and bilayer graphene properties was published by A. Mattausch and O. Pankratov [62]. In this study the electronic structure of graphene layers on 6H-SiC and features of the interface depending on the polarity were studied. It was found that in the case of graphene on Si-face, the first carbon layer (buffer layer) covalently bonded to SiC substrate is metallic, whereas on C face the interfacial layer is semiconducting. Only the second carbon layer was characterized by semi-metallic properties with Dirac cones in the electron spectrum. These authors underlined that the first carbon film acts as a buffer layer between the covalent SiC crystal and the van der Waals bonded stack of graphene layers [62].

Another relevant report dealing with the electronic structure of graphene layers on C-face and Si-face of 4H-SiC substrates was communicated by F. Varchon et al. [63]. The existence of strong covalent bonds between the substrate and the zero layer was confirmed by

x-ray reflectivity data [63]. It was shown that the first graphene layer is 1.65±0.05 Å above the last bulk carbon layer, whereas the next graphene layer is separated from the first by 3.51±0.01 Å. Due to the strong interaction between the substrate and the first graphene layer, charge transfer from SiC to graphene and formation of states in the vicinity of the Fermi level induced by interface intrinsic defects occur. These effects bring in lowering of the electronic mobility observed on Si-terminated surface and doping of the graphene layers. In particular, it was revealed that on the Si-terminated surface the Fermi level lies 0.4 eV above the Dirac point [63].

Most of the reports on the SiC face polarity effect up to now deal with a direct comparison between the properties of graphene grown on C-face and Si-face surfaces of 4H-SiC and/or 6H-SiC [35, 64-69], see also Table 1.

Table 1. Summary of literature data for graphene growth on different polar surfaces of silicon carbide by thermal decomposition

Substrate	**Growth conditions**	**Thickness**	**Properties**	**Ref.**
Si-face 6H-SiC C-face 4H-SiC	Gr/Si-face was grown by carbon evaporation under UHV at 950 °C during 30 min; Gr/C-face was obtained by heating at 1050 °C	1ML 1ML	Presence of interface layer with surface reconstruction in the case Gr/Si face For Si-face the Dirac point is shifted below the Fermi energy level by about 400 meV	[64]
Si-face 6H-SiC C-face 6H-SiC	Annealing in vacuum for 10–40 min at temperatures ranging from 1320°C	1ML 16ML	Sublimation occurs much more rapidly for the C face than the Si face so that 150 °C lower annealing temperatures are required for the C face to obtain graphene films; 3D formation of islands in the initial stage of graphene formation on C-face; Layer-by-layer growth of the graphene on Si-face in areas between the step bunches	[65]
Si-face 4H-SiC C-face 4H-SiC	UHV formation at 1500 °C for 10 min	2ML 8ML	Mobility: 4-29 $cm^2/V{\cdot}s$ vs. 24-530 $cm^2/V{\cdot}s$ for Gr/C-face vs. Gr/Si-face Step height for the Si-face was 0.5 nm Step height for the C-face was 1 nm The C-face graphene films are granular in nature resulting from an islanding growth mode; Si face graphene are smoother.	[66]
Si-face 4H-SiC C-face 4H-SiC	Radio frequency furnace annealing at 1500 °C for 10 min	4ML 45ML	Mobility: 1097-3462 $cm^2/V{\bullet}s$ vs. 77-477 cm2/V•s for Gr/C-face vs. Gr/Si-face;	[66]

			The C-face RF furnace films appear smooth, which may be the result of being thicker. Improvement in mobility is related to improving surface morphology	
Si-face 4H-SiC C-face 4H-SiC	High temperature annealing in vacuum at 1350 °C for 60 min	2ML 9ML	For Si-face growth: a grain size >5 μm with a rms roughness <0.5 nm; absence of disorder induced Raman D-peak; For C-face growth: presence grain boundaries and wrinkles, the grain size is ∼1 μm while the film roughness is ∼1 nm; rotational disorder;	[67]
Si-face 4H-SiC C-face 4H-SiC	Electron-Beam-Assisted Rapid Heating 2 min of e-beam irradiation	1ML 2ML	Uniform graphene layers with >70% coverage of single layer graphene on Si-face; Presence of voids and non-uniform layers with some defects C-face; FWHM of the 2D bands on the Si-face and C face are measured to be 21 cm^{-1} and 44 cm^{-1}; Hall Mobility: 3910 $cm^2/V•s$ vs. 6450 $cm^2/V•s$ for 2ML-Gr/C-face vs. 1ML-Gr/Si-face; Carrier Density: $3.8•10^{13}$ cm^{-2} vs. $1.5•10^{13}$ cm^{-2} for 2ML-Gr/C-face vs. 1ML-Gr/Si-face;	[43]
Si-face 6H-SiC C-face 6H-SiC	Annealing at 850 °C under or without a silicon flux for 2 min in UHV	2ML 2ML	The EG on C-SiC has a broader G band and stronger defect-induced D band, which means its crystallinity is worse than EG grown on Si-SiC; Due to difference of electronic structure, EG on C-SiC has much lower D and 2D-band frequencies, which are at 1343 and 2682 cm^{-1} compared to 1369 and 2736 cm^{-1} for EG on Si-SiC substrate;	[68]
Si-face 6H-SiC C-face 6H-SiC	Annealing in ultrahigh vacuum	1-2 ML 3-4 ML	On SiC (0001), the sequence of surface reconstructions observed during the graphene formation is (3×3), $\left(\sqrt{3}\times\sqrt{3}\right)R30^{\circ}$, $6\sqrt{3}$, and $(1\times1)_{graph}$. On SiC (000-1), the order of reconstructions is $(2\times2)_{Si}$, (3×3), $(2\times2)_{C}$, and $(1\times1)_{graph}$.	[35]
Si-face 3C-SiC C-face 3C-SiC	High temperature sublimation in Ar_2 atmosphere	1 ML 1-3ML	Large homogeneous domains with size up to $2·2mm^2$ are achieved on the Si-face, whereas the domains with smaller homogeneous thickness were obtained on the C-face; Due to smaller interaction of graphene with the C-face substrate the critical point energy for C-face graphene is higher than the respective values for graphene on Si-face;	[70]

Si-face 6H-SiC C-face 6H-SiC	Annealing in high vacuum environment for 60 min at 1350°C	2 ML 12 ML	Si-face growth is less dependent on the growth temperature C-face shows a significant increase in growth rate with temperature Si-face graphene with RMS roughness<0.5 nm and C-face graphene with RMS roughness ~1 nm.	[69]
Si-face 6H-SiC C-face 6H-SiC	Annealing at 1200 °C in vacuum	1.3ML 1.5-3.5 ML	In contrast to SiC (0001), graphene with smaller domain size grown on the C-face is not locked azimuthally to the substrate; The graphene growth rate and nucleation rate for C-face are significantly higher than on SiC(0001);	[44]
Si-face 6H-SiC C-face 6H-SiC	Thermal annealing over a temperature range of 1400 to 1450 °C with growth times varying from 30 to 60 min	2ML 5 ML	The RMS roughness for the Si-face graphene is 0.56 nm and that of the C-face graphene is around 0.67 nm; The lateral extent of the graphene domains could be smaller in the C-face graphene than in the Si-face graphene; Hall Mobility: 960 $cm^2/V•s$ vs. 1490 $cm^2/V•s$ for 5ML-Gr/C-face vs. 2ML-Gr/Si-face; Carrier Density: $2.8•10^{12}$ cm^{-2} vs. $4.6•10^{12}$ cm^{-2} for 5ML-Gr/C-face vs. 2ML-Gr/Si-face;	[71]

Experiments by Al-Temimy et al. [64] and by Ni et al. [68] suggest that the graphene growth on the (0001) surface of SiC substrates with different degree of hexagonality involves the formation of an interfacial layer with $\left(6\sqrt{3}\times 6\sqrt{3}\right)R30^\circ$ periodicity, as was confirmed by the corresponding first order graphene LEED spots surrounded by $\left(6\sqrt{3}\times 6\sqrt{3}\right)R30^\circ$ spots. At the same time, graphene growth on the C-face occurs immediately on top of the $\left(3\times 3\right)$ structure without the presence of an interface layer. However, LEED patterns of the graphene on the C-face surface demonstrate rings instead of spots developing at the first order diffraction angle of graphene. Such a picture is an indicator of a rotational disorder [35]. Similar results were obtained by V. Darakchieva *et al.* [70] for graphene on 3C-SiC (111) substrates (zero degree of hexagonality but still hexagonal face termination) with different face polarity.

As can be seen from Table 1, most of the graphene films on C-face are thicker than on Si-face and have smaller graphene domains. Luxmi et al. [65] propose that the difference in the graphene thicknesses on the C face and Si face is associated with the fact that the (000-1) face and (000-1)/graphene interface are more stable because they have lower energies than the (0001) surface and (0001)/graphene interface. In addition, it was reasonably assumed that more defects in the C-face films and/or rotational domain boundaries could lead to easier Si diffusion through the graphene, which would also favor thicker growth. This model agrees with the model proposed by B.K. Daas et al. [67]. These authors uncovered the nature of the thermodynamic

processes governing the growth mechanisms characteristic of each type of surface. The important role of defects in graphene formation was underlined. It was argued that only defect sites on the surface having free energy values higher than the surface can participate in the graphene growth process and can alter the step flow dynamics. Taking into account the fact that the surface free energy of the C-face is significantly lower than that of the Si-face, the number of possible defects sites participating in the growth process for C-face is much higher than for Si-face. Probably the latter is the reason for the existence of only one possible growth orientation ($\left(6\sqrt{3}\times 6\sqrt{3}\right)R30^{\circ}$ surface reconstruction) for Si-face graphene and multiple possible orientations for C-face graphene ($\left(2\times 2\right)$ and $\left(3\times 3\right)$reconstructions). It should be mentioned that the high rotational disorder and non-uniform stacking sequence in the case of graphene on C-face lead to a defect-induced enhancement of the growth rate and formation of thicker films. It means that the probability of the strain relaxation for C-face films is higher than for Si-face. In other words, for thicker C-face graphene films, greater than a critical thickness, strain relaxation typically occurs by the formation of a domain structure with large area of grain boundaries. Indeed, the AFM measurements obtained in Refs. [64, 67] confirm the presence of characteristic ridges and grain boundaries associated with strain relaxation. In this regard, the grain boundaries on the C-face promote Si out-diffusion from the SiC surface beneath the first graphene monolayers nucleated, causing the growth of multilayer films. On the other hand, graphene on the defect-free Si-face surface prevents the sublimation of the Si atoms underneath, thereby limiting the growth rate and graphene thickness.

2.1.2. Growth of graphene on Si-face SiC - growth kinetics, mechanisms and modes

For many years, the growth of epitaxial graphene on SiC substrates has been described through the mechanism that was firstly proposed by Badami [72]. It was experimentally revealed that the high-temperature heating of α-SiC (6H) single crystals in vacuum results in out-diffusion of silicon from the crystal lattice and the following reorganization of the two topmost layers of SiC. Such a change in the surface structure is responsible for the formation of one layer with the honeycomb arrangement of carbon atoms. In contrast to this, van Bommel [14] suggests that three topmost layers of SiC are needed to build up 1ML (one monolayer) graphene. This process was originally modeled by Kageshima et al. [73] by first principles approach. Fig. 4 illustrates 15 intermediate stages required for the formation of 1ML graphene. According to the authors' findings, the growth of the graphene sheet is a non- monotonic process. After the removal of a part of the Si atoms, carbon species can form not only different complexes and aggregates (such as monomers, dimers and trimers), but also can migrate to

silicon vacancies' sites and even substitute them. It was found that the most stable and favorable structure (from the energetic point of view) is 0-monolayer-graphene, the so-called buffer layer, that is partially covalently bonded to the SiC substrate. At the same time, the growth of the next graphene sheet (completely decoupled from the buffer layer) demands overcoming an energy barrier (which is approximately equal to 0.7 eV). The authors suggest that such a condition blocks further growth of the1ML graphene sheet. Overall, all of these features are characteristic of the interfacial growth mode. It should be also mentioned that this growth regime is strongly governed by surface diffusion processes and surface morphology of silicon carbide, which play a fundamental role in growing high-quality graphene layers [74]. In particular, surface morphology can be responsible for the strong nanostructuring of the interface carbon layer and even appearance of the so-called ripples [75], which may significantly influence the transport properties of graphene [76].

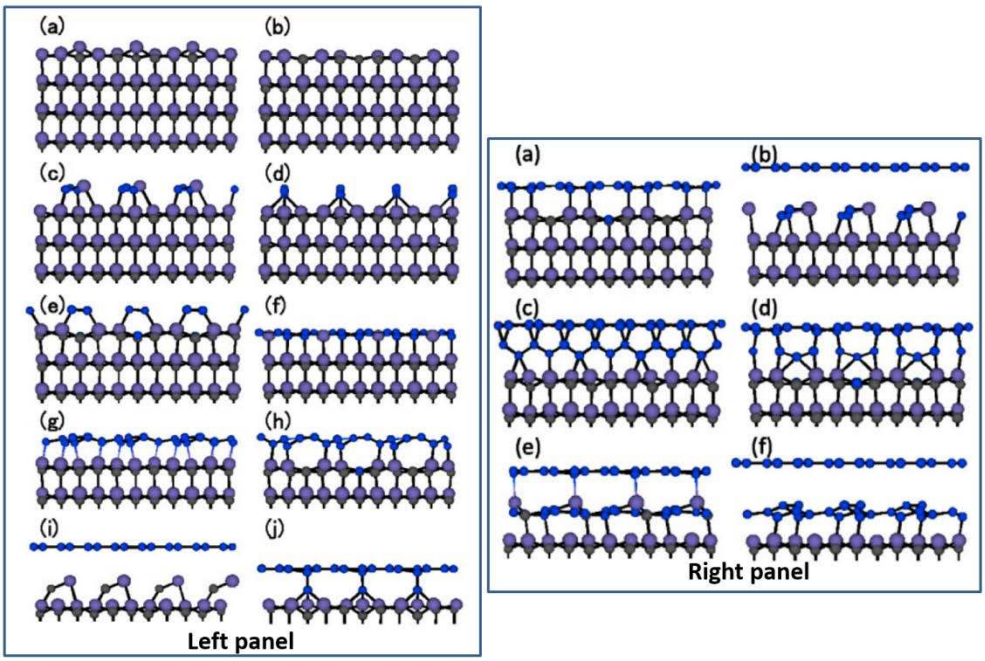

Figure 4. Different stages of Si evaporation from the SiC surface and graphene formation. Adapted from Kageshima et al [73]. Left panel demonstrates side views of the atomic structures with different number of removed silicon atoms, *n*. *n*=0 for (a) - *n*=9 for (j). Right panel illustrates the same, but from *n*=10 for (a) to *n*=15 for (f). Copyright (2015) AIP Publishing LLC

Using the advantages of the photoelectron holography, Matsui et al. [77] clearly demonstrated the formation of a buffer layer and the first graphene layer on top of a 4H-SiC(0001) substrate

at different thermal graphitization stages. As can be seen from Figure 5 the precursor ($6\sqrt{3}\times6\sqrt{3}$ R30° periodicity) layer and the buffer have the same local atomic configuration within the corrugation of 0–0.14 nm (see pink, blue, green and yellow circles). The red circles on the vertical cross section of this figure demonstrate the additional signal which appeared at the height of 0.33 ± 0.02 nm and those intensities are related to a single graphene layer.

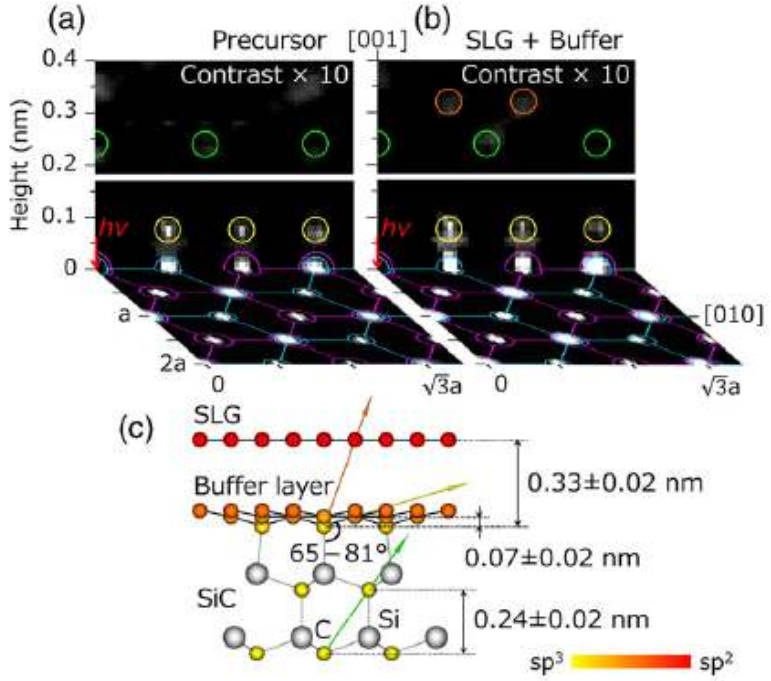

Figure 5. Reconstruction of three-dimensional atomic arrangements in the real space using the experimental full spherical C 1s photoelectron intensity angular distribution. Adapted from Matsui et al [77]. Copyright (2014) Elsevier B.V.

Combining the benefits of the Spectroscopic Photoemission and Low Energy Electron Microscope (SPELEEM), and Scanning Tunneling Microscopy (STM) techniques, Ouerghi et al. [78] proposed a model for the growth mechanism of graphene on 6H-SiC(0001). Fig. 6 illustrates the proposed mechanism. As can be seen from this figure, there are four main stages of graphitization in ultra-high vacuum conditions. During the first stage, intensive silicon sublimation through the most energetically favorable paths occurred. The horizontal diffusion path is related to the evaporation of silicon from the step edge, while the vertical diffusion path is associated with the movement of the silicon atoms from the bottom SiC layers through defect-containing regions of the interfacial carbon-rich layer (Fig. 6a). As a result of this anisotropic evaporation, randomly disturbed graphene flakes' formation takes place at the step edge (due to horizontal diffusion) and at the terraces (due to defect-related vertical diffusion), as shown in Fig. 6b. The third stage of the surface graphitization is followed by the propagation of the

step flow front toward the terraces' center and coalescence of the scattered flakes over terraces (Fig. 6c), and some additional sublimation of silicon atoms. Nevertheless, the vertical diffusion process is restricted to some extent. As a consequence, a decrease in graphene growth rate is observed. The authors explained such limitations by the inhibition of Si removal from the buried SiC decomposition front. It is reasonable to agree that the energetic barrier for Si sublimation increases after formation of the first graphene layer.

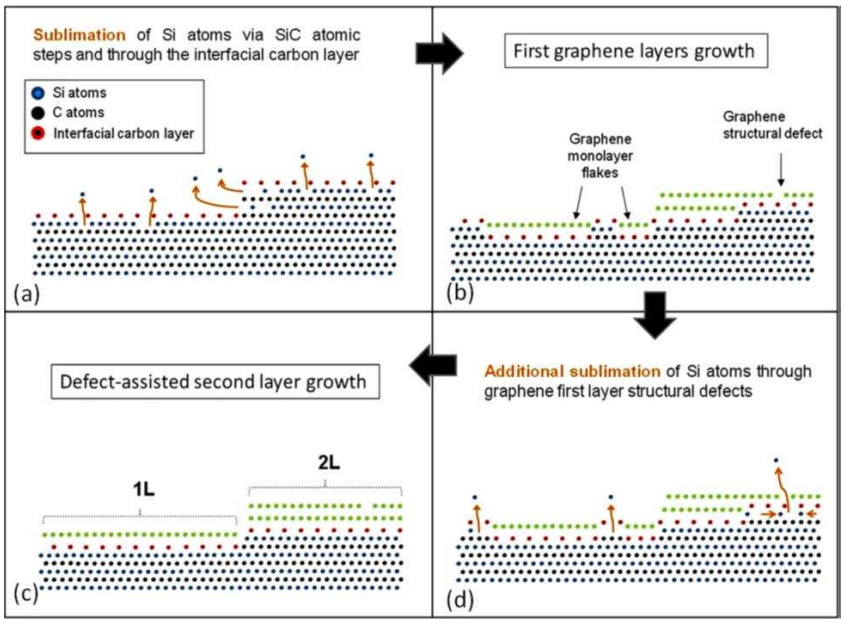

Figure 6. Illustration of the proposed mechanism. Adapted from Ouerghi et al. [78]. Copyright (2013) AIP Publishing LLC.

Another important step in understanding the growth modes of real graphene layers with consideration of the vicinal surface effect was done by Fan Ming [79]. The report by Fan Ming [79] has elucidated the nature of the growth kinetics of graphene on vicinal surfaces of Si-face SiC. This work presents the results of Monte-Carlo simulations showing how graphene nucleates and propagates at the step edge. In particular, the authors show the possible growth regimes. Fig. 7 represents the evolution of the kinetic processes for a vicinal surface of Si-face 6H-SiC which is composed exclusively of half-unit-cell- height steps. The first regime deals with the coalescence of strips occurring after nucleation of graphene at the steps while the second regime is associated with a "climb over" process that facilitates the propagation of graphene on terraces (from one terrace to the next). The authors also emphasized that the "climb over" processes tend to make graphene surface more inhomogeneous.

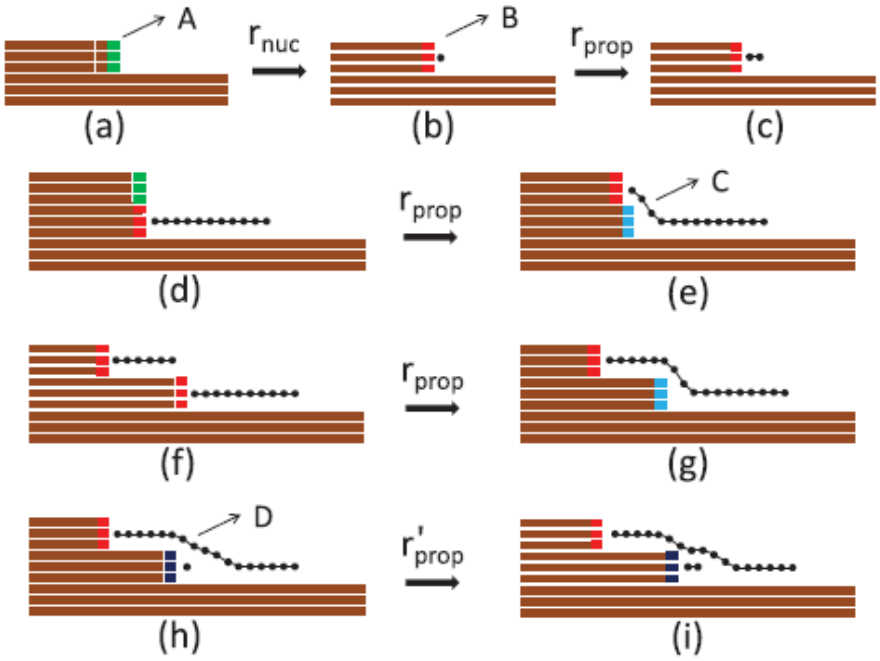

Figure 7. Evolution of the growth kinetics for graphene onto vicinal surfaces of silicon carbide. Adapted from F. Ming et al. [79]. Copyright (2011) American Physical Society.

In an earlier study, with the aid of adsorbing cobalt (Co) in the role of a tracer, it has been possible to map the transformation of the carbon-rich reconstructed surface to a monolayer and few layer graphene on a 6H-SiC (0001) substrate [80]. It has been demonstrated that the graphene formation begins from the step edges terminated with double dangling bonds. Immediately after, due to the high-temperature annealing the Si-C bonds within the reconstructed layer tend to be broken and graphene formation occurred. At the same time, the three layers of the bulk structure of 6H-SiC (with ideal stacking sequence) underneath the buffer layer are involved in the formation of a new reconstructed buffer layer beneath the graphene one. The original sketch of the growth mechanism is illustrated by Fig. 8. However, this result contradicts with the finding by Tang et al. who reported on two carbon-rich layers required for formation of graphene [81]. It has been also predicted by the kinetic theory that graphene formation occurs with an energy barrier of ~3.0 eV, suggesting that the breaking of the Si–C bond is most likely to be the rate-limiting step in the transformation of the reconstructed surface to graphene (because this value of energy barrier is close to Si-C bond energy of 3.3 eV) [80]. It was concluded that when the surface of SiC (mainly the surface reconstruction) has few defects, the idea of obtaining large-scale high-quality graphene can be realized since there is a direct correlation between size/quality of reconstructed surface and size of graphene domain. Our own experimental results are in full agreement with these findings. The reason for the

success in understanding growth of high-quality epitaxial graphene on 6H-SiC is that the 6H polytype has a great advantage over others since its intrinsic stacking promotes the formation of reconstructed surface naturally after removing the first 3 SiC bilayers [80]. This has been demonstrated for graphenation of 6H-SiC in various studies [82-85]. Among them, by magnetotransport measurements on Hall bar devices, Yager *et al.* show wafer-scale homogeneity of transport properties in epitaxial graphene on 6H-SiC [83].

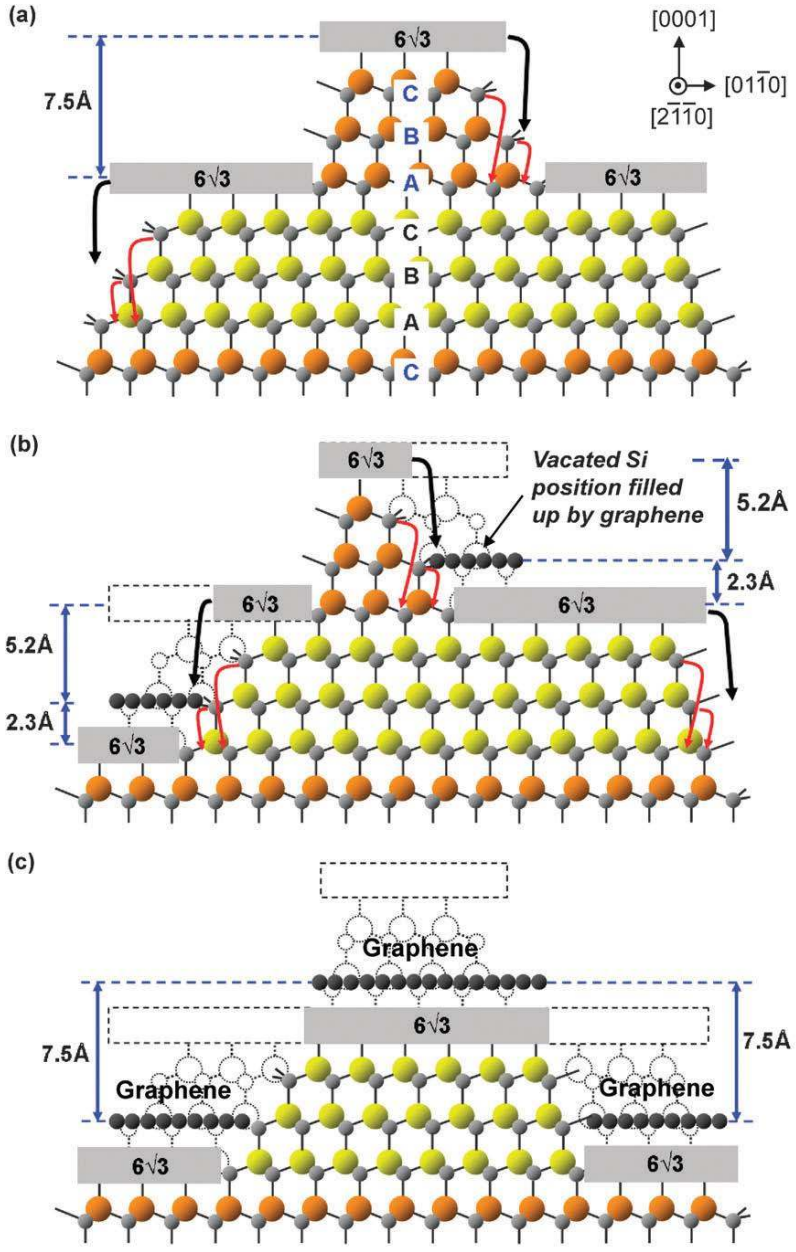

Figure 8. Schematic of the growth mechanism of 1MLepitaxial graphene. Orange and yellow filled circles correspond to Si species, whereas dark grey balls represent C atoms. Adapted from F. Poon et al. [80]. Copyright (2010) The Royal Society of Chemistry.

It is interesting to note that Wang et al. [86] demonstrated a novel approach to optimize graphene growth on 6H-SiC (0001) associating it with so-called dynamic flip mechanism. The model illustrating this mechanism is presented in Figure 9. This method is based on the fact that Si sublimation occurs easier from a surface Si cluster (Si-Si bonds) than via breaking the sp^2 and sp^3 bonds between carbon and silicon (Si-C bonds). In particular, flipping the Si-C bond has been found to lead to the formation of a surface Si cluster (Si-Si bonds) and carbon cluster in the second layer. Such transformations are favorable for graphene growth. At the same time, the energetic barrier for flipping the Si-C bond is rather high (5.6 eV) and requires sufficient thermal energy to be overcome. Nevertheless, the authors suggest that the participation of Si vacancies in the flipping events has been found to lead to lowering this barrier from 5.6 eV to 2.4 eV. According to the authors finding, the graphitization occurs via the following stages: (1) generation of silicon vacancies (energy barrier is ~7-8 eV); (2) vacancy-assisted Si-C bond flipping (energy of 2.4 eV); (3) Si sublimation from the surface cluster composed of mainly Si atoms and Si-Si bonds (energy of 5.5-5.7 eV); (4) propagation of Si sublimation and reorganization of C atoms into graphene; and (5) decoupling of graphene layer from the SiC substrate. It should be emphasized that this work demonstrated the feasibility of the energy-controlled growth of graphene layers at much lower temperatures in comparison to conventional thermal heating in argon atmosphere.

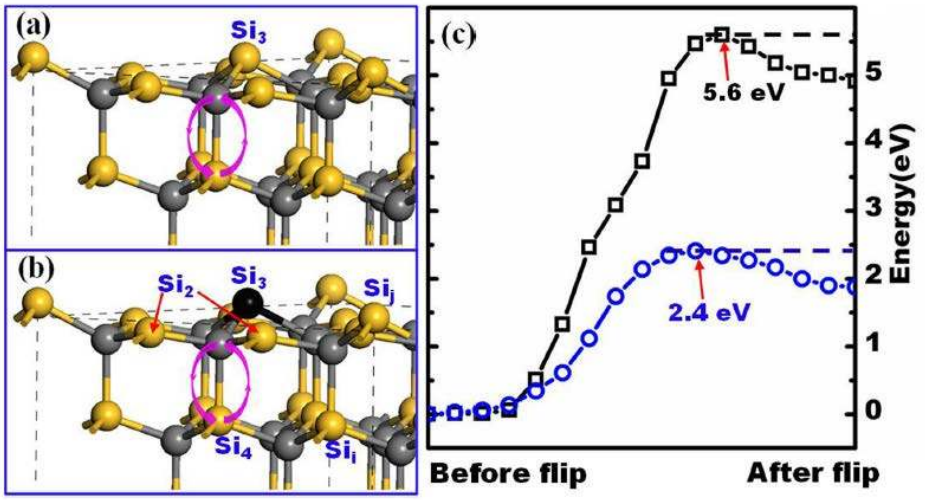

Figure 9. Models showing the bond flip processes on (a) defect-free and (b) in the presence of a Si vacancy created by sublimation of Si_3, respectively, of the $(\sqrt{3}\times\sqrt{3})R30^\circ$ reconstructed surface, and (c) the corresponding minimum energy paths (black square for model (a) and blue circle for model (b)). The black ball indicates the Si vacancy created by sublimation of Si_3. The

pink arrows show schematically the exchange of the Si-C pairs. Adapted from Wang *et al.* [86]. Copyright (2015) Royal Society of Chemistry.

Nontrivial approach to reduce the graphitization temperature was also suggested in Ref. [87]. Zhang et al. synthesized graphene layers on 6H–SiC with reduced graphitization temperature via ion implantation [87]. In particular, it was shown that, in virtue of electronic and nuclear collisions, ion implantation by energetic Ar, C_1 and C_6-cluster ions can cause breaking of the Si–C bonds, thereby promoting the appearance of an additional carbon source. Overall, such an approach allows lowering the graphitization temperature by 200°C.

While 6H-SiC shows more natural to promote easy graphene formation, the 4H – SiC technology of semiinsulating crystals and wafer surface preparation is more advanced because of the demands from the SiC based device manufacturers. For example, the wafer size increases faster and the wafer surface is basically scratch-free. For these reasons many graphene researchers have focused on this polytype. W. Strupinski et al. [88] fabricated graphene on semi-insulating on-axis 4H- SiC substrates cut out from a 4 inch wafer. The formation mechanism of graphene was investigated using Micro-Raman and SEM studies. It was shown that the Si sublimation causes the formation of a carbon buffer layer having a large number of point defects related to sp^3 bonding (10% of sp^3 hybridization). The distance between these sp^3 defects was estimated to be as large as 10–15 Å. The authors revealed that the silicon sublimation from the vicinity of macro-step edges is more favorable, thereby supplying additional free carbon atoms for the buffer layer. Certainly,

Important role of the surface defects in graphene growth was revealed by Park et al. [89]. The authors purposefully created an extended surface SiC-like defected layer on the SiC substrate prior to growth of graphene. This defected layer strongly influenced graphene formation. In particular, using such defected layer for graphene formation gives rise to a reduction of surface pits in the samples. It is possible to control the graphene thickness via controlling the properties of this defected layer. Park and co-workers give a sensible explanation of the observation of pit-free surfaces for graphene on defected on-axis 4H–SiC (0001) wafers [89]. It is well known that the migration of SiC steps via gaps on the terraces in the C-rich buffer is responsible for pit nucleation [90]. In their turn, Park et al. suggested that the surface carbon in the defected SiC layer can prevent the migration of SiC steps, thereby blocking pit formation [89]. Furthermore, it has been also revealed that during the formation of the 0^{th} graphene layer, the steps can be energetically stable and non-reactive [91]. However, using defected layers for graphene growth has its own bottleneck because of an increased compressive strain. This strain

leads to the formation of many wrinkles along and across the terraces and, consequently, to a shift of the Raman G and 2D bands [89]. Therefore, a trade-off must be reached between defects' number and graphene quality. Similar defect-induced strain in graphene samples was also observed in Ref. [92] for graphene on 6H-SiC(0001).

J. Osaklung et al. [93] reported on enhanced graphene growth on 6H–SiC(0001) surfaces having scratches. In contrast to well-known "step edge" graphene growth mechanism, the graphene formation occurs not only above scratch areas but also extended from both edges of the scratch. It can be explained by the fact that a scratch has a wedge shape rather than a step shape (Figure 10).

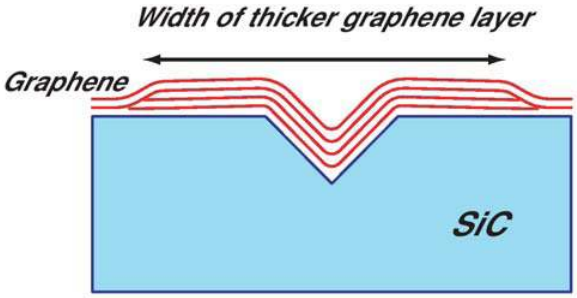

Figure 10. Sketch of the graphene growth mechanism on scratched SiC surface. Adapted from J. Osaklung et al. [93]. Copyright (2012) Elsevier B.V.

As was reported by A. Ruammaitree et al. [94], a defect-mediated mechanism is also responsible for the formation of non-concentric graphene rings and triangle-shaped graphene islands. In particular, these graphene rings start to grow from the SiC hexagonal pits induced by carbon vacancies. In other words, when the carbon vacancy is formed, the sublimation of Si atoms becomes much easier due to a decrease in the number of sp^3 bonds with the surrounding Si atoms. Immediately after, the next outer carbon atoms are involved in the same process, thereby leading to the formation of an initial hexagonal SiC pit with zigzag-edge on the terrace and new pit inside the old one. A schematic representation of this mechanism is showed by Figure 11. Vectors in Fig. 11a indicate that edge step erosion of the larger pit is faster than of the smaller one, since the erosion of the pit step depends on the step height. As a result of the step erosion, free carbon species can form graphene layer between the large and small pit area following the conventional step edge mechanism (Fig. 11b). As demonstrated in Fig. 11(c), this process continues until the graphene surrounds completely the small pit. Furthermore, as was concluded that the difference in the erosion rate, because of the SiC stacking fault (possessing different number of dangling bonds on the steps) and independence of the erosion of two pit edges leads to a formation of triangle-like shape of graphene islands (Fig. 11(d)).

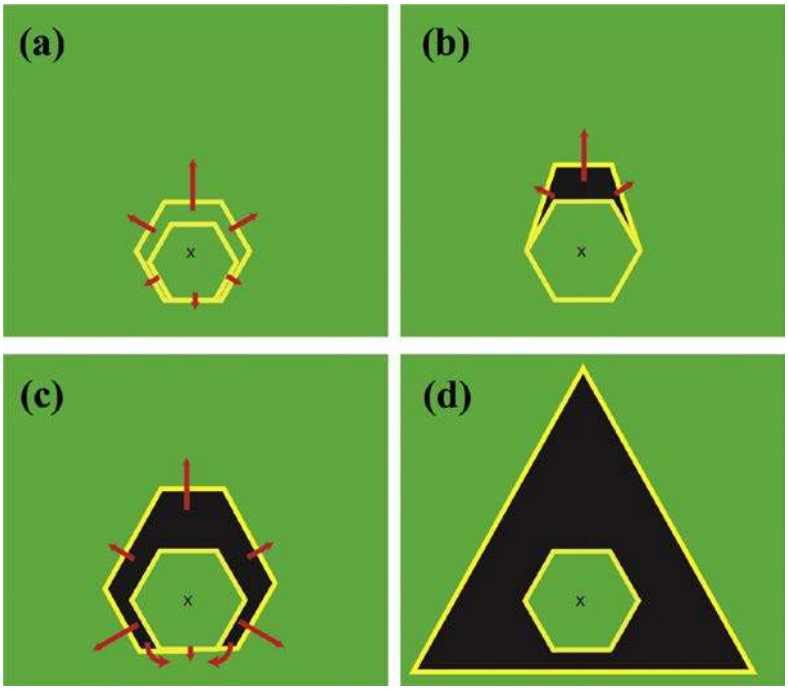

Figure 11. Illustration of the formation of graphene rings and triangle-shaped graphene islands. Green and black colored areas represent the SiC and graphene. Adapted from A. Ruammaitree et al. [94]. Copyright (2014) Elsevier B.V.

As opposed to the aforementioned graphene growth on defective SiC surfaces, A.N. Hattori et al. [95] reported on the formation of graphene films on damage-free and atomically flat 4H-SiC(0001) surfaces. It is reasonable to assume that growth of graphene on damaged and rough SiC surface is accompanied by an increasing of the silicon desorption rate and, as a consequence, an appearance of a lot of carbon nucleation centers limiting the graphene domain size. Strictly speaking, increasing the domain size requires necessity to overcome the activation barriers between different nuclei. Thus, growth of graphene layers on damaged surfaces demands high-temperature annealing in order to achieve good quality graphene. A.N. Hattori et al. [95] showed that using atomically flat SiC surfaces can promote more uniform Si desorption and graphitization processed. As a result, graphene layers with wide domains may be prepared at lower temperatures.

2.1.3. Effect of the SiC substrate on the growth of graphene - off-axis, non-polar planes and polytypism

Future integration of graphene with SiC technology for developing new-generation electronics platform demands using not only high-quality free-standing graphene, but also high-quality epitaxial SiC layers. Commonly used on-axis SiC substrates suffer from the formation of 3C–SiC inclusions and/or polycrystalline areas in the SiC epitaxial layer grown on top and, as a consequence, are problematic for graphene growth [96]. As opposed to this, off-axis substrates prevent this problem and give a possibility to obtain high-quality SiC epilayers. In particular, 4° and 8°off-axis 4H–SiC (0001) substrates are the standard platform of current SiC technology for power electronics [97]. In contrast to graphene layers grown on on-axis (0001) and (000-1) SiC substrates, where a general consensus on the growth conditions and mechanisms was achieved, unconventional features of the graphene layers grown on vicinal surfaces are not yet well understood, since the misorientation angle (called also tilt-angle, or miscut angle, or off-axis angle) can play a significant role in the graphene formation [98]. It is due to the strong sensitivity of the growth rate to the structural features of the terraces and steps characteristic of the off-axis surface. Indeed, in the case of vicinal surfaces the kinks of the SiC terraces can be nucleation sites of graphene growth [98]. It can cause an enhancement of the growth rate in comparison to growth on terraces of on-axis SiC substrates in virtue of reduced spacing between the terrace kinks [98].

Another important challenge on the way to the successful integration of graphene with silicon carbide is the necessity to choose an appropriate polytype the SiC substrate. Since each polytype is characterized by an unique stacking sequence, one may expect not only a difference in growth kinetics of graphene on different polytypes of SiC, but also a strong dependence of the electronic properties (carrier mobility, carrier density, doping scenario) of graphene on the degree of SiC hexagonality (in virtue of the sensitivity of spontaneous polarization of the SiC to the kind of polytype). For the same reason, it is also very important to find out how graphene grows on non-polar surfaces of SiC and how one may tune its properties by playing with the type of the SiC surface.

In this section we review the current status of graphene formation on: off-axis and nonopolar SiC surfaces with a primary focus on the miscut angle and nonpolar surface effect on the properties of graphene and growth mechanisms. Furthermore, we highlight the role of the SiC polytypism in growth of graphene.

One of the main problems faced in growing graphene layers is a high thickness non-uniformity. In earlier investigations, the formation of a large-area continuous 1ML graphene sheet on 6H-SiC (0001) substrates with low miscut angle (0.03° towards [1-100]) was achieved [84]. In contrast to this graphene, where full coverage of the terraces (~6 μm width) and steps

(<15Å height) was observed, graphene on 0.25° tilted-off axis SiC was either in the form of long ribbons or large non continuous sheets (due to the impossibility to determine the covering of 40-50Å high steps) [84]. Kajiwara et al. [99] experimentally confirmed the formation of densely ordered arrays of epitaxial graphene nanoribbons on vicinal 6H-SiC substrates (Si face, 4° off toward [1-100]). J. Penuelas *et al.* [100] disclosed the growth mechanism of graphene on *n*-type Si-terminated 6H-SiC(0001) (on 3; 5° off). It was revealed that the graphitization starts from the step edges and propagates gradually to the center of the terrace. In this case, the carbon atoms at terrace kinks and step edges have a lower coordination number, thereby leading to an easier breaking the bonds at these sites. For this reason, the probability of SiC decomposition and further surface diffusion of carbon atoms is increased and a graphitization of the SiC surface occurs. Similar growth mechanism was reported by Camara et al. [96] for graphene on 8° off-axis 4H–SiC (000–1) substrates. In this case, however, a presence of single layer graphene islands having triangular shape was observed. It was concluded that the growth starts from one nucleating center and expands in a two-dimension carpet-like mode. The graphene obtained in this way was strain-free (according to Raman studies) and was characterized by a hole concentration n_s=1.2·10^{12} cm^{-2} and a mobility 5000 cm^2/V·s at T=1.6 K. Kisoda et al. [101] found a great shift of the Raman G-peak to a higher frequency for graphene on 4° off-axis 6H–SiC (0001), which means the presence of in-plane compressive stress induced by the substrate. It was suggested that the compressive stress can be completely relaxed within five to six graphene layers. Tanaka et al. [102] revealed anisotropic layer-by-layer growth of graphene on 6H-SiC substrates (Si-face, 4° off toward [11-20]). A growth mechanism including three different stages was proposed [102]. The first stage is represented by the formation of a buffer layer and nucleation of monolayer graphene on the (11-2n) nanofacets, followed by 1 ML graphene growth over the entire surface. During the second stage, the nucleation of a second graphene layer at the nanofacets below the first graphene layer and a continuous graphene growth via layer-by-layer mode occurs. And finally the last stage is similar to the second one except that the graphene thickness has increased. Nevertheless, these authors did not clarify whether the buffer layer is present at the nanofacet area. Concomitantly, F. Giannazzo et al. [98] revealed the absence of the interfacial C buffer layer on (11-2n) nanofacets. These features lead to anisotropy of the channel conductance with respect to the steps' orientation. In particular, scanning probe microscopy-based local electron mean free path measurements on epitaxial graphene showed a three-fold enhancement of the mean free path on the buffer-layer-free (11-2n) facets in comparison to (0001) terraces. It can be explained by

the strong reduction of Coulomb scattering effects on graphene's electrons at the nanofacets' regions.

Another group [103] reported atomic-scale transport in epitaxial graphene grown on misorientated Si-terminated 4H SiC substrates with off-cut angles 0.06° and 0.5°. Similarly to [84] it was found that the sample with the low miscut angle has a larger fraction of monolayer graphene than that with the high miscut angle. The authors emphasized that the macroscopic conductivity measurements give a possibility to estimate only a small part of the full picture required to gain insight into the transport through graphene on SiC. In particular, miscut related steps, islands formed during the growth process and thickness inhomogeneity can be responsible for the reduction of the macroscopic conductivity. To support these statements the authors measured both local conductivity on single terraces and macroscopic conductivity. It was revealed that in the case of graphene grown on high-miscut SiC the macroscopic conductivity was three times lower than the local value, whereas the graphene on low-miscut SiC showed a difference of only by 1.2. It can be explained by the dramatic potential jumps at the step edges, and a potential gradient on the terraces. For example, it was measured that the monolayer graphene crossing single substrate steps with height 0.5 nm shows a resistance of 6.9±2.9 Ohm·μm. The increase of the step height from 1 nm to 1.5 nm leads to increase in the resistance from 14.9±3.6 Ohm·μm to 24.7±4.3 Ohm·μm. At the same time, monolayer-bilayer junctions have a higher resistance, 20.9±5.7 Ohm·μm and 28.4±7.0 Ohm·μm for graphene covering terrace and crossing the step edge, respectively. Nakatsuji et al. [104] showed that graphene at the substrate step edge is curved for the samples grown on Si-terminated surfaces of nitrogen-doped 6H- and 4H-SiC(0001) substrates that were tilted with 4° and 8° toward the [1-100] direction. Such features eventually lead to a change in the group velocity along Γ-K-M in the direction of graphene deformation and elongation of the Dirac cone as was measured by angle-resolved photoelectron spectroscopy (ARPES). In this scenario, the value of the group velocity in the direction parallel to the [1-100] (step-down) direction is smaller than that in the other K-M directions. Under such conditions, graphene on the 8°-off SiC surface with high step density has a smaller value of the group velocity and a high anisotropy than that on the 4°-off SiC with a lower step density. For graphene on 6H-SiC(0001) substrates tilted toward the [11-20] (4° off), it was observed that the spectrum in the direction perpendicular to the step-down direction has a narrower width in the momentum distribution than the band in the other direction for 0 eV$<E_B<$0.2 eV [104].

Hupalo et al. [105] give a deep insight into the physical nature of the graphene formation mechanism on vicinal 6H-SiC(0001) surfaces. In particular, these authors suggested that there

are several competing kinetic processes which govern the graphene growth. One of them is related to Si desorption through steps and others are associated with the necessity to reach tradeoff between carbon diffusion rate and island nucleation. The most important finding is an experimental observation of the anisotropy of the Si desorption rate. In other words, different SiC steps have different evaporation rates [105].

The effect of the miscut angle on the morphological and electrical properties of graphene was investigated by Dimitrakopoulos et al. [106]. It was observed that the width of terraces in each case is inversely proportional to the miscut angle. Interestingly to note that for miscut angles above 0.28° the surface under graphene is pit-free or minimally pitted, whereas below 0.10° a higher density of larger and deeper pits appears. A direct correlation between terrace width and carrier mobility was revealed. Graphene films grown on 4H and 6H-SiC substrates with high misorientation angles and smaller values of terrace width demonstrate a lower carrier mobility compared to those with low miscut angles. Probably it can be understood in terms of carrier mean free path. When the average terrace width is similar to or smaller than the mean free path, the carrier mobility is reduced and vice versa. At the same time, the role of pits on the carrier transport was found to be minimal.

Robinson et al. [107] studied graphene transport and structural properties depending on the Si-face 6H-SiC wafer orientation. According to the AFM study and Raman 2D/G ratio, it was found that miscut angles ≥0.2° lead to the formation of uniform, parallel steps consisting of (0001) terrace flats and (11-0n) terrace edges. In this case, graphene on the terrace center and edge is a monolayer and bilayer graphene. In addition, increase in the miscut angle causes an enhancement of the terrace edge density, thereby leading to an increase in graphene thickness at this region. A strong sensitivity of the carrier transport to the misorientation angle was observed. In particular, the average carrier density increases and carrier mobility decreases with increasing the miscut angle from 0.02° to 1.25°.

Table 2 below summarizes literature data on the thickness of graphene on Si-face SiC substrates with different miscut angles by using different growth techniques.

Table 2. Summary of literature data for graphene growth on off-axis surfaces of Si-face SiC

Substrate	Growth Conditions	Miscut angle	Thickness	Ref.
4H-SiC	Electron-beam heating at 1300 °C	0.06°	1-2ML	[103]
4H-SiC	Electron-beam heating at 1300 °C	0.5°	1-2ML	[103]
6H-SiC	Annealing in 5×10^{-6} Torr N_2 gas at 1970 K, typically for 1 s	4°	1.05 ML	[104]
4H-SiC	Annealing in 5×10^{-6} Torr N_2 gas at 1970 K, typically for 1 s	8°	1.20 ML	[104]

6H-SiC	Annealing in UHV at 1200 ºC with heating step of 30 s	0.005rad	1-2 ML	[105]
6H-SiC	Annealing in UHV at 1500–1600K for 3min	3.5°	3-4ML	[108]
6H-SiC	Annealing in UHV or N2 gas over 1900 K for up to a few hundred seconds	4°	1ML	[104]
4H-SiC	Thermal annealing Ar at 900 mbar at 1700°C	8°	1-2ML	[98]
6H-SiC	Annealing in UHV at 1500 °C during 15 s	4°	1-1.5ML	[106]
6H-SiC	Annealing at temperature of 2000°C and at an ambient argon pressure of 1 atm	0.03°	1ML	[84]
6H-SiC	Annealing at temperature of 2000°C and at an ambient argon pressure of 1 atm	0.25°	1-2ML	[84]
6H-SiC	Synthesis at 1625 °C for 15 min in an argon-mediated background pressure of 1 Torr	0.02°-1.25°	1-2ML	[107]
6H-SiC	Graphenizing at 1550 °C for 10 min under Ar flow at a chamber pressure of 3.5 mTorr.	0.02°-1.25°	2±1ML	[106]
6H-SiC	Surface graphitization at 1600 °C for 10 min	4°	1-3ML	[102]
6H-SiC	Annealing in UHV at 1300°C under a base pressure lower than 10^{-9} mbar	3; 5°	2ML	[100]
6H-SiC	Solid state graphitization technique at 1400°C	4°	1.8-3ML	[101]

As mentioned before, the growth of graphene layers on polar SiC surfaces brings in the appearance of a carbon-rich buffer layer with $\left(6\sqrt{3}\times 6\sqrt{3}\right)R30^{\circ}$ periodicity that is partially bonded to the substrate. This interfacial layer leads to degradation of the electronic properties of graphene (because of high-electron doping) and limitation of the carrier mobility (due to scattering mechanisms induced by substrate). In this regard, it is very important to provide quasi-free-standing graphene growth with reduced buffer layer effect. Recently, it was discovered that the graphitization process of non-polar SiC surfaces leads to direct growth of quasi-free-standing graphene without a buffer layer [109, 110]. M. Ostler et al. [109] reported the electronic and structural properties of graphene layers grown on the low-index $\left(11\bar{2}0\right)$ and $\left(1\bar{1}00\right)$ 4H-SiC surfaces using sublimation growth in an Ar atmosphere. In contrast to graphene on polar SiC surface, XPS C1s spectra of nonpolar surfaces are characterized by the absence of the component related to the buffer layer. Macro-LEED measurement confirmed the formation of a quasi-free-standing graphene. At the same time, there is some difference between two non-polar surfaces. Graphene on $\left(1\bar{1}00\right)$ SiC surfaces demonstrates high degree of rotational disorder and high thickness non-uniformity, whereas graphene/$\left(11\bar{2}0\right)$ SiC grows without rotational disorder, with more uniform large-area ML graphene coverage [109]. This difference can be understood in terms of geometrical and topological features of each non-polar configuration. As was shown by Ostler et al. [109] the first relaxed graphene layer on SiC$\left(11\bar{2}0\right)$ is flat and non-corrugated. At the same time, the first graphene layer on $\left(1\bar{1}00\right)$SiC surface has a corrugation with amplitude of about 0.3 Å.

Daas et al. [67] investigated the growth modes of graphene on non-polar 6H-SiC, on both *a*-plane $(11\bar{2}0)$ (EG-a) and *m*-plane $(1\bar{1}00)$ (EG-m) faces. It was demonstrated that, under the same growth conditions, both EG-a and EG-m were thicker than those of their corresponding polar *c*-plane samples and have poorer surface morphology with surface roughness values of ~3 nm. The authors correctly assumed that the poorer morphology of the EG-a and EG-m compared to EG-c is caused by the lack of a clear hexagonal template, as well as the differences in surface energies and step dynamics of the substrate surface. Furthermore, Raman characterization revealed a larger I_D/I_G ratio on the nonpolar faces compared to the polar faces, thereby suggesting higher disorder in graphene films on non-polar surfaces and smaller values of in-plane coherence length. The principle difference in graphene growth modes between polar and nonpolar surfaces was also explained in Ref. [67]. It was concluded that the graphene growth on the polar face proceeds laterally while the graphene growth on the nonpolar *a*-plane and *m*-plane faces is limited by the vertical growth rate. Such a complicated vertical growth produces scattered islands of epitaxial graphene on the surface with higher density of grain boundaries. The latter causes a greater amount of Si out-diffusion from the substrate, leading to a thicker subsequent multilayer graphene growth on the nonpolar faces. In addition, it was found that graphene growth on the lowest packed *m*-plane face is faster than that of the high densely packed *a*-plane. It is generally accepted that the high surface density limits the graphene growth rate, not promoting Si sublimation and requires more time for the formation of in-plane C−C-bonds and larger grains. A complicated nature of the graphene growth on the non-polar *m*-plane and *a*-plane 6H-SiC was also uncovered in Refs. [111, 112], where the authors observed a multilayer graphene formation with a high degree of rotational disorder and Moire´ patterns of different spatial periodicities. Lin et al. [113] studied the domination carrier scattering mechanisms for the graphene grown on 6H-SiC substrates with nonpolar orientations $(1\bar{1}00)$ and $(11\bar{2}0)$. It was revealed that the interaction between substrate and film is minimal in the case of the $(1\bar{1}00)$ surface, thereby leading to a dominating scattering mechanism originating from defects in graphene layer. At the same time, the substrate scattering mechanism is dominant for the graphene on $(11\bar{2}0)$ surface. However, the sample on $(11\bar{2}0)$ has larger carrier mobility than that on $(1\bar{1}00)$.

In contrast to the common trend when only non-polar faces of hexagonal 4H and 6H polytypes were used for graphene growth, P. Hens et al. [110] developed a new approach for graphene growth using thermal decomposition of (001)-oriented cubic silicon carbide. Absence

of a buffer layer and presence of two domains in the layer rotated by approximately 30° was shown. Table 3 below summarizes literature data on growth features of graphene on non-polar planes of SiC by using different growth techniques.

Table 3. Summary of literature data for graphene growth on non-polar planes of silicon carbide

Substrate	**Growth Conditions**	**Thickness**	**Properties**	**Ref.**
$(1\bar{1}00)$ 4H-SiC	Sublimation growth in an Ar atmosphere	2.0 ± 0.1 ML	Large rotational disorder; Large thickness nonuniformity	[115]
$(11\bar{2}0)$ 4H-SiC	Sublimation growth in an Ar atmosphere	2.0 ± 0.1 ML	Absence of rotational disorder; Uniform graphene coverage	[116]
$(1\bar{1}00)$ 6H-SiC	Thermal decomposition in vacuum (10^{-6} Torr) during 60 min at 1350°C	16ML	Grain size ~30 nm	[68]
$(11\bar{2}0)$ 6H-SiC	Thermal decomposition in vacuum (10^{-6} Torr) during 60 min at 1350°C	12ML	Grain size ~70 nm	[68]
$(1\bar{1}00)$ 6H-SiC	Thermal decomposition during 15 min under a flowing Ar environment of 20 standard liters per min. at 100 mbar, at 1620 °C.	3-4 ML	Roughness of 0.62 nm; Average step height of 2.5 nm; Rotational disorder; Moire´ patterns;	[117]
$(11\bar{2}0)$ 6H-SiC	Thermal decomposition during 60 min under a flowing Ar environment of 20 standard liters per min. at 100 mbar, at 1620 °C.	3-4 ML	Twisted graphene with a rotation angle of 5.4°	[118]
(001) 3C-SiC	High temperature graphene process during 20 min at 1800 °C at argon gas pressure of 800 mbar	1-3 ML	Domain sizes of a few micrometer Dirac point located within 0.2 eV from the Fermi level	[116]
$(11\bar{2}0)$ 6H-SiC	Physical vapor transport (PVT)	5-6ML	Smooth surface Hall mobility:2028 $cm^2/V\cdot s$ Carrier density: $18\cdot10^{12}cm^{-2}$	[119]
$(1\bar{1}00)$ 6H-SiC	Physical vapor transport (PVT)	5-6ML	Rough surface Hall mobility:1685 $cm^2/V\cdot s$ Carrier density: $44.7\cdot10^{12}cm^{-2}$	[119]
$(11\bar{2}0)$ 6H-SiC	Annealing during 60 min at 1400°C	20ML	Crystalline coherence length: 60 nm High denstity of defects Nanocrystalline graphite like features	[71]
$(1\bar{1}00)$ 6H-SiC	Annealing during 60 min at 1400°C	28ML	Crystalline coherence length: 40 nm High denstity of defects Nanocrystalline graphite like features	[71]

Earlier works dealing with study of graphitization mechanisms for SiC polytypes were motivated by the desire to determine the most favorable surface for graphene growth [114]. Yakimova *et al*. [115] reported the effect of the SiC polytypism on the morphological and

electronic properties of graphene layers. A principle difference in the thickness nonuniformity of graphene layers grown on hexagonal (4H and 6H) and cubic (3C) SiC substrates by Si sublimation at high temperatures was found. Such a difference was reasonably explained by the difference in the specific step height distribution and different energetics of the existing terraces in the three polytypes [115]. Among all polytypes the 3C-SiC substrate is desirable for growth of uniform epitaxial graphene layers due to only one kind of steps and minimization of the detrimental role of step bunching [116]. The polytypism effect clearly manifests itself also in the electronic properties of the graphene films [115, 117]. The critical point energy in the dielectric function related to van-Hove singularity for graphene on 3C-SiC was smaller (4.33 eV) than that of graphene on 4H-SiC (4.55 eV) and 6H-SiC (4.40 eV) [115].

C. Coletti et al. [118] experimentally showed that the band velocity of trilayer graphene on 6H-SiC (0001) is smaller than that on 3C-SiC ($0.93 \cdot 10^6$ m/s vs. $1.05 \cdot 10^6$ m/s). Such a difference can be ascribed to a dependence of the Fermi velocity on the substrate [119].

Another important aspect is that the kind of polytype significantly affects the type of conductivity of graphene layers [120]. It is a common knowledge that the morphological properties of graphene layers and degree of interaction between the graphene layer and the SiC substrate determine the doping level of the graphene layer. It was theoretically predicted that graphene/3C-SiC (111) samples demonstrate *n*-type conductivity, whereas the graphene on the 6H- and 4H-SiC(0001) samples are *p*-doped [120]. The bulk spontaneous polarization occurring in particular SiC polytype is considered as a source of doping [120]. The authors of Ref. [120] studied the impact of the polytype, respectively the related spontaneous polarization, on the carrier density of hydrogen intercalated graphene prepared on 6H-, 4H-, and 3C-SiC. It was clearly stated that the 3C-SiC substrate induces the least doping. The effect of SiC hexagonality on the electronic properties of graphene layers was experimentally studied in Ref. [121, 122]. It was shown that the intrinsic doping level in bilayer graphene grown on 6H-SiC(0001) substrates is lower than on 4H-SiC(0001) [121]. This is suggested to be due to a difference in the spontaneous polarization of the substrate materials. Mammadov *et al.* [122] reported experimental evidences of polarization doping of quasi-free-standing graphene on different polytypes of the silicon carbide (namely 6H-, 4H, and 3C-SiC). By using angle-resolved photoelectron spectroscopy (see Figure 12), the authors revealed that the Dirac point in the case of graphene grown on hexagonal 6H- and 4H-SiC substrates is positioned above the Fermi level, thereby indicating the *p*-type conductivity. Furthermore, there is a direct correlation between the magnitude of the spontaneous polarization and the doping level. In particular, 4H-SiC having a larger spontaneous polarization than that of 6H-SiC induces a larger

hole concentration. As can be also seen from Figure 12, an absence of the spontaneous polarization in cubic (3C) polytype causes a negligible *n*-type doping in the quasi-free-standing graphene, which is mainly originating from bulk doping. The authors concluded that 3C-SiC polytype can be regarded, in principle, as a substrate promoting the smallest carrier concentration in graphene.

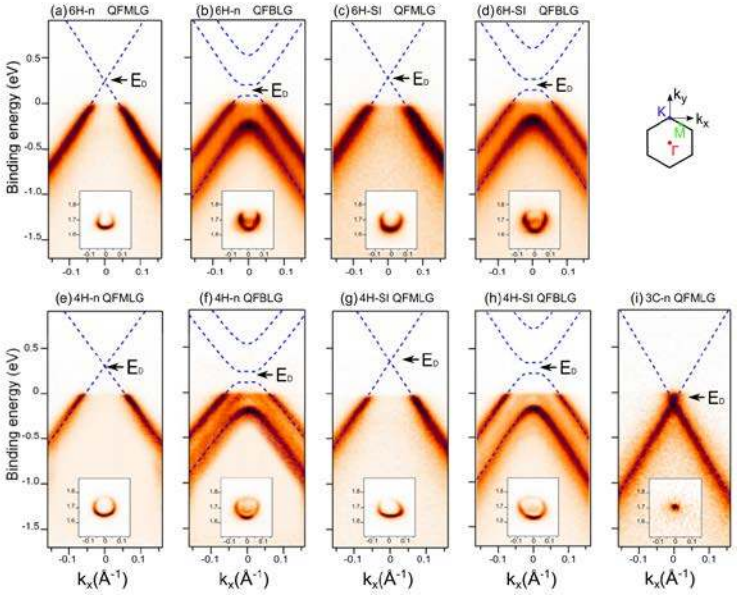

Figure 12. ARPES intensity maps measured for quasi-free-standing monolayer graphene (QFMLG) and quasi-free-standing bilayer graphene (QFBLG) on (a), (b) n-type 6H-SiC(0001), (c), (d) semi-insulating 6H-SiC(0001), (e), (f) *n*-type 4H-SiC(0001), (g), (h) semi-insulating 4H-SiC(0001) and (i) *n*-type 3C-SiC(111). Adapted from Mammadov *et al.* [122]. Copyright (2014) IOP Publishing Ltd.

2.2. Growth of graphene on SiC using external sources.

It is essential to appraise chemical vapor deposition (CVD) and molecular beam epitaxy (MBE) in this review since these are the most popular techniques in micro- and nano-electronics in general. Both represent the bottom-up growth approach and imply the necessity of using external sources of carbon (solid, liquid or gaseous carbon sources) to form graphene layers. The substrate, in this case, is expected to play more passive role compared to the SiC sublimation technique. There is a lot of excellent reports in literature dealing with deposition of graphene from external sources on metallic surfaces (Cu, Ni, Ir, etc) and on dielectric wafers (SiC, sapphire, Si, etc.). Following the main purpose of this review paper, we focus only on the CVD and MBE growth of graphene on silicon carbide [114, 121, 123-141]. Therefore, the aim of this subsection is twofold: (i) to understand the main difference between thermal

decomposition of silicon carbide and bottom-up growth of graphene on SiC and (ii) to extensively review the literature concerning the CVD and MBE growth processes with participation of SiC substrate. It should be noted that while CVD growth of graphene on metals is well established, the process on SiC started its development not so long ago. The main concern is to avoid formation of a buffer layer when the substrate is exposed to a high temperature (>1200 ºC). Recently, progress in this direction has been made, e.g. see Ref. [123].

In order to gain insight into the variance between the different approaches of graphene growth on SiC, we depict two main graphene growth strategies: (i) thermal decomposition and (ii) deposition from external sources. As can be seen from Figure 13a the thermal decomposition of the Si-face SiC substrates refers to a special case of top-down growth process of graphene. In particular, this method implies that the graphene is synthesized by erosion of several topmost crystalline planes, which are present on the substrate and by a subsequent self-assembling the "popping up" carbon atoms into a planar sp^2 graphene surface. Hence, the top-down approach implies that the part of the topmost layers of SiC substrate must be removed to allow the graphene layers to be formed from the lying beneath carbon atoms. It is generally accepted that the graphene layers obtained in this manner are considered as epitaxial or quasi-epitaxial. It is important to note that the definition "epitaxial" is only nominal, since we do not deal with the classic epitaxial growth like in the top-down approach. The term "epitaxial" in this case is mainly associated with the fact that the strong covalent interaction between the C-rich interfacial layer and SiC ensures an epitaxial relationship between the reconstructed surface of the SiC substrate and the graphene sheet.

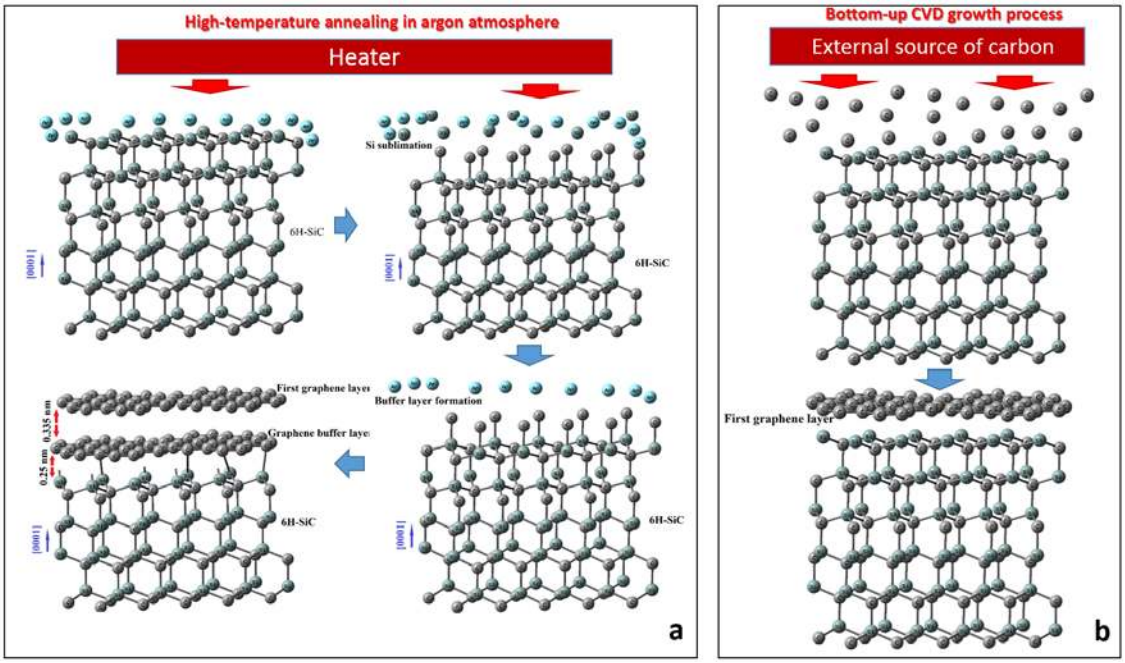

Figure 13. Visualization of the top-down (a) and bottom up (b) growth strategies of graphene layers on Si-face SiC substrate considering intermediate stages. Top-down process is proper to the thermal decomposition approach and represents the situation when erosion of the SiC substrate occurs from “top” to “down” thereby freeing the carbon atoms that can participate in the graphene formation. Bottom-up approach is represented by the CVD process and is not related to disintegration of the substrate.

The bottom up approach does not imply the necessity to consume the surface of the SiC substrate and is mostly related to deposition of carbon atoms on the SiC surface (or eventually other substrates) from an external source (Fig. 13b) and subsequent self-organization of the incoming carbon adatoms on the SiC surface into graphene. While the sublimation growth of graphene is a top-down process, the bottom up process infers that the carbon-containing building blocks are added onto the SiC substrate by stacking carbon atoms onto each other, thereby forming the graphene sheet.

K. Grodecki et al. [123] studied the difference between the two processes. Such a difference was explained in terms of growth kinetics. In the case of the thermal decomposition approach, the graphene formation starts mainly at step edges and different surface defects are directly involved into this process. In fact, these randomly distributed defects are responsible for the pining of the graphene layer to the SiC substrate. Indeed, during the sublimation silicon atoms below the buffer layer cannot have an easy possibility to pass through the buffer layer and probably search more favorable places for out-of diffusion and evaporating (for instance defects related to the pinning points). The authors suggested that such vertical silicon diffusion from the bottom SiC layer through the topmost graphene layers can lead to a strong pinning of the graphene to the substrate. In contrast to this approach, the CVD technique offers some additional advantage due to the fact that the carbon atoms condense directly on the substrate from an external supply and graphene nucleation most likely occurs on flat terraces. In these conditions, the vertical silicon diffusion (sublimation process) is mostly blocked and smaller number of pinning points is expected. Thus, the graphene layers grown in this manner are unpinned from the SiC substrate. This is evidenced by the measurements of the thermal shift rate of the 2D Raman line. Low sensitivity of the Raman 2D peak to change of the temperature is peculiar to free-standing graphene and indicates an unpinning of epitaxial graphene.

Bearing in mind the difference between top-down and bottom-up growth processes, it is important to emphasize that bottom-up growth of epitaxial graphene layers is more versatile in comparison to sublimation technique. This is due to the possibility to use lower temperatures

for graphene formation, to control more variable growth conditions and to provide more easily doping scenario for graphene. In principle, these advantages can play a key role in the light of future applications of epitaxial graphene. Therefore, it is necessary to understand deeply what is going on during bottom-up growth and to elucidate the nature of the self-assembling of graphene by interaction of the SiC surface with incoming carbon-containing molecules. Although CVD growth of graphene can be realized by using a wide range of carbon sources, the principle of specificity dictates that some carbon-containing substances will promote better quality of graphene than others. The most widely studied among the carbon sources is propane [114, 121, 124, 126, 128-137]. There is only a few works devoted to ethene [125], toluene [127] and xylene [127] as carbon sources for graphene growth on silicon carbide.

Probably, the first results on CVD growth of graphene on SiC were reported by Hwang *et al.* [135]. In particular, the indications of graphene formation on C-face on-axis 6H–SiC substrate by the propane-assisted CVD process were experimentally demonstrated by using Raman characterization (graphene-related G, 2D and D peaks were detected). In order to show that the graphene formation is not caused by silicon sublimation, the authors reported that CVD process in argon atmosphere without propane flow under the same conditions did not lead to formation of graphene (no characteristic Raman peaks were observed). The strong sensitivity of the graphene quality (thickness, domain size and number of defects) to the growth time, propane flow rate and growth temperature allows the authors to conclude that: (i) increasing the growth temperature is responsible for the increasing the domain size, (ii) formation of graphene starts after 2 min (nucleation time) and (iii) graphene growth is not possible at a low propane flow (there is some critical value of the propane flow rate, which is required for nucleation of the graphitic carbon films). Using the same technique and the same external carbon source W. Strupinski *et al.* [128] reported on the graphene epitaxy by CVD on C- and Si-faces of on-axis 4H-SiC substrates. The authors emphasized that the most important factor enabling graphene formation following the CVD growth mechanism is the ratio between the Si sublimation temperature and the critical pressure of argon. Strictly speaking, graphene growth is only possible under specific conditions promoting mass transport and/or diffusion of the carbon-containing molecules (propane) to the surface of the silicon carbide and preventing the Si sublimation. The formation of argon boundary layer with critical thickness blocks the silicon evaporation from the SiC surface, thereby satisfying the abovementioned conditions. As a result of such kinetic processes, only the molecules of propane can diffuse through argon boundary layer. Immediately after, these hydrocarbons are thermally decomposed and available carbon atoms directly deposit on the SiC surface and take part in formation of the sp^2-bonded graphitic

carbon layer. More detailed study of the growth modes of graphene synthesized by argon–propane assisted CVD on 3C–SiC/Si and 6H–SiC can be found in Ref. [134]. Similarly to Hwang's report [135], these authors investigate how the graphitic phase covers the SiC surface depending on the CVD process duration. In particular three different stages were revealed: (i) a latency period during which the carbon supply and deposition rate are very low; (ii) a second period associated with beginning of the graphene phase nucleation and (iii) a third period characterized by a drastic increase in graphene thickness. The authors reasonably assume that only the deposition regime during the CVD process is responsible for graphene formation and the difference in the deposition rates at the different growth stages can be explained by the changes of the surface energy. Indeed, the surface of SiC during the initial growth stage is carbon-poor. It means that its surface energy is higher in comparison to that of graphitic phase and therefore graphene forms via a 2D growth mode. When the surface of SiC becomes carbon rich, the surface energy is lowered in comparison to the graphitic phase and the transition from 2D growth mode to 3D one occurred. Due to this reason the graphene coverage is not continuous and homogeneous (even separate graphitic clusters can be formed). A possibility to synthesis monolayer graphene on 6H-SiC (0001) by propane-argon assisted CVD technique at the temperature of 1600 ºC was demonstrated by K. Gajewski *et al.* [133]. Graphene layers grown in this manner were corrugated. According to the results of the scanning tunneling microscopy (STM) measurements the authors conclude that Moiré pattern is present and a surface reconstruction is caused by interaction of the CVD graphene and a buffer layer beneath. Such growth features are responsible for the non-homogeneous electrical properties of monolayer graphene. The important role of structural and morphological properties of the 4H-SiC surface in the growth mode of the graphene layers was shown in Ref. [137]. In particular, it was revealed that due to a step bunching induced by both etching in hydrogen and process of the graphene formation, the graphene grown by using an external carbon source (propane) and carrier gas (argon) is characterized by stepped morphology. Because of the difference in growth kinetics, the graphene on terraces is thinner, more homogeneous with a smaller level of strain fluctuations in comparison to the graphene on step edges. It leads to the fact that the electronic properties (for example, carrier concentration) are not the same for graphene on terraces and graphene on the step edges.

Although the exact mechanisms of propane-assisted CVD growth of graphene on SiC have not been fully elucidated, it is believed that the SiC surface demonstrates a significant catalytic effect in the adsorption process of propane molecules [124]. In this context, the theoretical calculations, which were done by M. Wierzbowska *et al.* [124], gain insight into the

nature of the CVD formation of graphene in argon atmosphere by means of propane gas as a carbon source. As was shown in this work, two main chemical processes that govern the graphene formation are adsorption of the propane molecules and dehydrogenation. Figure 14 summarizes the optimized geometries describing the adsorption events of the propane and transition C_3H_{8-n} (n=1…8) species. It is important to noted that due to the fact that all chemical bonds in propane molecule are saturated, the C_3H_8 molecules weakly interact with the SiC surface (unbound state). In order to enhance this interaction, some part of the hydrogen atoms should be removed (as can be seen in Fig. 14). To explain the dehydrogenation process the authors predicted the possibility of formation of ArH^+ charged molecules via the binding reaction of a proton to argon. The authors claimed that the main factor that is required for the formation of the carbon adlayer is the deprotonization on the SiC surface in argon atmosphere. This is associated with the existence of ArH^+ molecules and negative charge transfers from the adsorbates to the SiC surface. Thus, the graphene epitaxy by the chemical vapor deposition process occurred with direct participation of SiC surface as a strong catalyzer that promotes the dehydrogenation process.

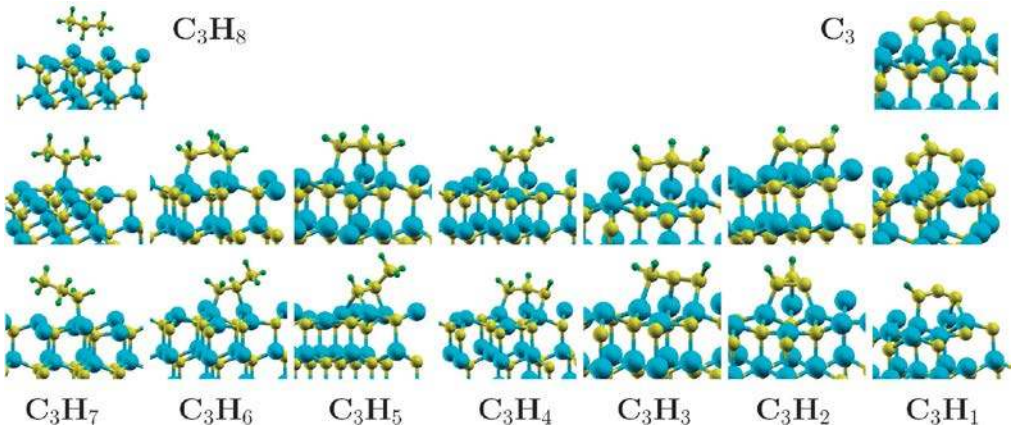

Figure 14. Optimized geometries showing the interaction between propane and transition C_3H_{8-n} (n=1…8) species with SiC surface. Adapted from M. Wierzbowska et al. [124]. Copyright (2015). The Royal Society of Chemistry

Up to this moment we considered only the literature reports devoted to propane-argon assisted growth, but there is also some interesting experimental data on CVD growth of graphene by using hydrogen as a carrier gas [114, 126, 129, 131, 132, 136]. Michon *et al.* [114, 126, 129] demonstrated the possibility of direct growth of graphene on 6H-SiC (0001) and 3C-SiC/Si substrates. It was concluded that the increase in propane flow in propane-hydrogen gas

mixture leads to a significant decrease in the SiC etching rate and increase in graphene thickness. It is important to note that the main advantage coming from using hydrogen as a carrier gas is related to the fact that hydrogen can saturate the dangling bonds of silicon at the substrate interface, thereby preventing the formation of the so-called buffer layer covalently bonded to SiC and, as a consequence, the charge transfer from SiC substrate to graphene. This assumption was evidenced by (i) absence of buffer layer-related spots and peaks in the LEED patterns and XPS spectra, respectively; and (ii) observation of rotational disorder (which is usually observed for graphene layers on C-face of the SiC substrate, without a buffer layer). Therefore, hydrogen-related growth factor is often referred to as the most important technological factor promoting the desired intercalation of graphene during the CVD process. It is thought to provide a saturation of the dangling bonds and formation of a quasi-free-standing graphene. Meanwhile, the behavior of the hydrogen during the CVD process is temperature-dependent [107]. In other words, in the low temperature regime the probability of the formation of Si_{SiC}-H covalent bonds is higher than that of the Si_{SiC}-$C_{graphene}$ bonding and thus no buffer layer is observed [129]. It was reasonably assumed that the hydrogenation of the SiC surface starts before the graphene formation. On the other hand, in the high temperature regime the formation of the Si_{SiC}-$C_{graphene}$ covalent bonds seems to be more preferred thus causing interface reconstruction (some part of carbon atoms of graphene can bind to the substrate). Michon et al. [126] attempt to uncover the physical nature of the graphene growth mechanisms using the propane-hydrogen CVD process on 6H-SiC (0001) substrates depending on the growth pressure and growth temperature. It was supposed that different technological growth regimes regulate the competition between different kinetic processes, which are responsible for the carbon supply and graphene formation. Among them the most important are: (i) participation of the carbon atoms coming from the propane flow in self-assembling of graphene, (ii) hydrogen-induced SiC chemical etching providing an additional carbon source for graphene formation, and (iii) diffusion of carbon-containing molecules from the surface of SiC substrate to the gas phase. It is interesting to note that all these processes are involved in graphene formation via a surface reconstruction (buffer layer). At the same time, the carbon-containing adsorbents (mostly from propane flow) are only responsible for the formation of the buffer-free graphene with rotational disorder.

Reports on the synthesis of graphene on SiC by using other carbon sources are limited by Refs. [125, 127]. Cai et al. [125] studied ethene-argon assisted CVD growth of graphene on C- and Si-face 4H-SiC substrates. The graphene growth on both planes was driven by changing the chamber pressure. In the case of Si-face, increasing the growth pressure from 1 mbar to 100

mbar leads to transformation of the graphene surface from stepped to smooth morphology. While for the C-faced 4H-SiC, the picture is completely different. In particular, the growth at the 100 mbar leads to forming rough surface morphology with uneven distribution of the irregular terraces. Similarly to epitaxial graphene on Si-face SiC, a decrease in the chamber pressure to 1 mbar is responsible for the appearance of the stepped surface morphology of graphene (with unobvious and irregular steps). From the discussion above and analysis of the Ref. [125], one can conclude that the mechanisms describing the ethene-assisted growth of graphene on SiC are not understood yet and their understanding demands further investigations.

Unusual approach to graphene synthesis on 4H-SiC by CVD method by using a liquid carbon sources (xylene and toluene) was reported by Kim *et al.* [127]. Overall, the xylen- and toluene-mediated growth mechanisms are governed by the completion between such kinetics processes as collision and diffusion of the incoming species on the SiC surface, absorption, dehydrogenation and formation of the graphene nuclei. It is interesting to note that using toluene-based liquid source gives rise to the formation of epitaxial graphene, whereas utilizing xylene as the liquid carbon source leads to synthesis of graphene oxide. The observation of the characteristic Raman peaks is a clear indication of the formation of graphene and graphene oxide on SiC substrate, respectively. Such a difference in growth kinetics can be explained by the fact that the toluene and xylene on the SiC surface behave themselves in a different manner. Toluene is characterized by a stronger absorption energy, lower activation energy and lower dehydrogenation energy in comparison to xylene. Furthermore, due to the fact that xylene has more methyl groups than toluene, the bond-breaking energy is increased and the reactivity of xylene is limited. For these reasons, the graphene growth in the presence of xylene is, to a large extent, unattainable and only graphene oxide is formed. According to the authors' findings, the toluene-based graphene has the characteristic hexagonal structure, whereas the formation of the xylene-based graphene oxide is accompanied by agglomeration of a nanometer-sized needle-like graphene structure.

Another important method employing external C source for deposition of graphene on SiC is molecular beam epitaxy (MBE). There is only a few works devoted to MBE growth of graphene namely on silicon carbide [99, 138-141]. In contrast to the CVD technique where carbon-containing gases or liquids decompose at high temperatures to form graphene, the MBE growth implies using high purity carbon sources (pure carbon flux) to obtain graphene layers. In principle, such approach should allow to avoid the dehydrogenation stage (in virtue of the absence of the typical C-H bonding in hydrocarbons) and provide homogenous graphene nucleation over large areas. Moreau *et al.* experimentally showed that MBE process gives a

possibility to grow high-quality graphene layers on carbon-faced 6H-SiC [138] and 4H-SiC [139] substrates. It is important to note that surface morphology of graphene deposited in such manner repeats the step-terrace structure of the initially treated SiC surface, thereby indicating that MBE process do not lead to erosion or degradation of the SiC surface. The observed rotated domains and stacking of rotated graphene planes are typical for graphene on C-face SiC. In addition, authors reported on the possibility to control precisely the graphene thickness. At the same time, the question about the exact growth mechanism and kinetics is still open. To gain insight into the physical nature of graphene formation during the MBE process, Razado-Colambo investigated the stacking of graphene layers on the C-face of 4H-SiC [141]. The presence of the two types of graphene domains rotated with respect to the SiC substrate was unambiguously demonstrated. The first kind is consisting of AB stacked multilayer grains, whereas the second one can be mainly attributed to the twisted bilayer or single layer graphene.

To get better understanding of the MBE growth of graphene, Moreau *et al.* [139] also used the Si-face 6H-SiC as a substrate and revealed that the graphene layer is rotated by 30º with respect to the SiC. XPS peaks typical for the interface between SiC substrate and graphene layer are detected, thereby suggesting the presence of an interfacial layer. In contrast to previous reports, Kajiwara *et al.* [99] offered to use the silicon-faced vicinal surfaces (4◦ off toward [1-100]) of 6H-SiC for MBE growth of graphene nanoribbons (10 nm in width). It was reported that using vicinal surfaces with high miscut angles promote the selective growth of graphene. In particular, the self-assembling of the incoming carbon atoms mainly occurred at the (0001) terraces and is virtually absent at the (1-10n) nanofacets. At the first stage of the growth procedure, the buffer layer is formed on the terraces and then after the hydrogen intercalation this interfacial layer transforms to quasi-free-standing graphene. Meanwhile, it is not fully understood what is the physical reason for such selective growth and why graphene phase is not formed on the nano-facets.

2.3. Alternative approaches to graphene synthesis on SiC.

Several different approaches have been proposed to decrease the growth temperature, for example, Ni-induced graphene formation [142-149], segregation method using Co/SiC system [150-152], catalytic alloy approach [153] and Ga-mediated liquid phase growth [154, 155]).

To solve the growth temperature problem, Juang *et al.* [142] proposed to use nickel as a catalytic metal for the formation of millimeter-scaled monolayer graphene on 6H–SiC (0001) and 3C–SiC coated Si substrates. The thickness of the Ni film was chosen to be 200 nm. The matter is that the thermal annealing of the Ni/SiC structure leads to inter-diffusion and, as a

consequence, to the formation of a mixed phase (to be more exact, nickel silicide/carbon) with further diffusion of the carbon atoms to nickel. Subsequently, owing to the low solubility of carbon in nickel, carbon atoms segregate on the Ni surface and then self-assembling of the popping-up atoms into graphene occurred. All these processes are possible at quite low temperature (750 ºC). The schematics of this process is illustrated by Figure. 15.

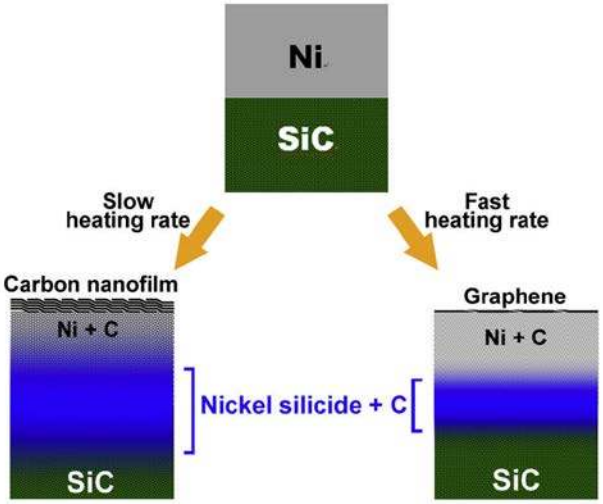

Figure 15. Sketch of the Ni-mediated graphene formation on SiC. Adapted from Juang *et al.* [142]. Copyright (2009) Elsevier Ltd.

It is important to note that graphene growth mechanism in this case is mainly regulated by the heating rate, since both the fraction of the nickel silicide phase and the number of segregated carbon atoms, which are available for graphene formation, depend strongly on the heating rate. Indeed, low values of the heating rate cause the increase in the nickel silicide fraction and, therefore, more carbon atoms are available for graphene nucleation (and vice versa for high heating rate regime). Noteworthy the authors did not reveal any effect of the SiC polytypes (3C or 6H) on the low temperature Ni-mediated graphene growth and assumed that this growth mechanism is not sensitive to the polytype of the SiC substrate.

Following the Ni-mediated carbon segregation approach, different groups reported on successful synthesis of graphitic films. A summary of the literature data is presented in Table 4.

Table 4. Summary of literature data for Ni-mediated growth of graphene on SiC substrates

Substrate	**Growth conditions**	**Ni film thickness**	**Graphene properties**	**Ref.**
6H-SiC 3C-SiC/Si	Annealing of the Ni/6H-SiC and Ni/3C-SiC/Si at 750 °C	200 nm	Formation of the single-layer large-area graphene films	[142]

6H-SiC	Annealing of the Ni/6H-SiC at 700 °C	0.4-50 nm	Strong dependence of the graphene morphology on the Ni film thickness At the thickness of 0.4 nm, uniform carbon-overlayer is formed. At the thicknesses of 0.6–9.6 nm, clustering and platelet formation are observed At the thickness of 50 nm, the hillocks are occurred	[143]
C-face 4H-SiC	Annealing of the Ni/4H-SiC at 1100 °C for 300 sec	5, 20 and 100 nm	At the Ni thickness of 5 nm, the solid graphitic film is formed At the Ni thickness of 20 nm, continuous graphene film occurs. At the Ni thickness of 100 nm, graphene films consists of separated domains	[144]
C-face 6H-SiC Si-face 6H-SiC	Growth via Ni-silicidation reactions in UHV for 5 min at 950°C and 1000°C for C-face and Si-face, respectively	5 and 10 ML	Double layer graphene with work function of 4.25±0.05 eV is formed on the Si-face Single layer graphene with work function of 5.15±0.05 eV is formed on the C-face	[145]
Si-face 6H-SiC	Annealing of the Ni(200 nm)/SiC structure at 1080 °C for 10 s	200 nm	Graphene film consisting of 3–4 carbon monolayers is formed	[146]
Si-face 6H-SiC	Growth via Ni-silicidation reactions in UHV with the temperatures of 600, 700, 800, and 950 °C	5 nm	Graphene film consisting of 3–8 carbon monolayers is formed at different temperatures; Optimized annealing temperature is about 800 C.	[147]
Poly-crystalline SiC powders	Selective solid-phase chemical reactions between Ni and poly-crystalline SiC powders at the temperature of 1000 °C	-	Graphene consisting of 1–3 layers with microns in size was grown	[148]
C-face 6H-SiC Si-face 6H-SiC	Local solid phase growth from nickel silicide supersaturated with carbon at temperatures ranging from 700 °C to 1080 °C	3-20 nm	Patterned few layer graphene films with carrier Hall mobilities of 50 $cm^2 \cdot V^{-1} \cdot s^{-1}$ and sheet concentrations of 10^{13} cm^{-2} were grown Strong sensitivity grown films to the technological parameters	[149]

Yoneda et al. [145] and Escobedo-Cousin et al. [149] reported the significant meaning of the face polarity effect for the Ni-mediated process. It was revealed that the thickness of C-face graphene (1ML [145], 1.7ML [149]) is smaller than that of Si-face graphene (2ML [145], 3.3ML [149]). Such a difference can be explained by a faster reaction rate for Ni with the Si–C bilayer than with the C–Si bilayers [145]. It leads to a more efficient electronic charge transfer between thicker graphene films on the Si-face and SiC substrates than that between the thinner

C-face graphene and SiC. It was shown that the binding energy value of C 1s for the 1ML-graphene/SiC(000-1) is larger by 0.5 eV than that for the 2ML-graphene/SiC(0001) [145].

To elucidate the nature of the Ni-mediated graphene growth mechanism on silicon carbide, Escobedo-Cousin *et al.* [149] experimentally studied the effect of the different growth conditions (Ni layer thickness, annealing temperature, and cooling rate) on the graphene formation. Based on the results of the XPS and Raman characterization, these authors conclude that (i) slowing the cooling rate leads to the formation of graphene layers with higher quality, (ii) higher annealing temperature promotes graphene formation with larger domain size and (iii) there is no a direct correlation between graphene thickness and Ni film thickness since the former tends to reach saturation with increasing the latter. The authors reasonably assumed that such unusual dependence of the number of graphene layers on the Ni layer thickness can be explained by the fact that only a part of the segregated carbon atoms (among all available C species) participate in graphene formation process. A sketch of the growth mechanism describing the Ni-assisted formation of graphene on silicon carbide is illustrated in Fig. 16. As can be seen from this sketch, the authors distinguish four separated growth stages underlying the Ni-mediated growth of graphene on a silicon carbide substrate. First stage (Figure 16a) represents the initial situation dealing with pre-deposition of the Ni film on the SiC surface. During the second stage (at growth temperatures exceeding 600 ºC), due to a chemical reaction between nickel and silicon, a mixed phase occurred, thereby forming the reaction zone consisting of nickel silicide, Ni_2Si, and carbon atoms (Figure 16b). Then thermodynamics and kinetics of the growth is governed by the presence of two diffusion flows in opposite directions. One of them is associated with movement of the Ni atoms towards the SiC substrate to maintain the silicidation reaction. Another one is related to diffusion of the carbon atoms in the Ni layer and further segregation of the carbon on the Ni surface. A fraction of the available carbon atoms participate in self-assembling of the graphene layers. In principle, after the second stage the thermodynamic mechanisms, which are dependent on the carbon solubility in nickel and Ni film thickness, can prevent further growth of the graphene (Figure 16c). The final stage of the growth process (Figure 16d) is mainly regulated by cooling the system. In particular, it was suggested that the decrease in temperature causes lowering of the carbon solubility in nickel silicide. Due to this reason the Ni_2Si phase becomes supersaturated and graphene formation or occurrence of precipitates are possible.

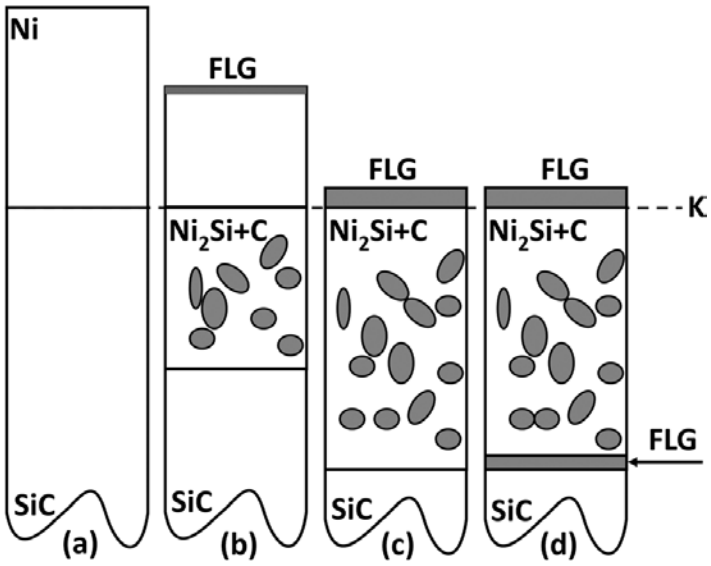

Figure 16. Illustration of the mechanism underlying the growth of the graphene films with participation of nickel as s catalytic metal. FLG denotes few-layer graphene. Adapted from Escobedo-Cousin et al. [149]. Copyright (2013) AIP publishing.

Another approach involves the use of cobalt as a catalytic metal to form graphene layers and to lower the growth temperature [150-152]. Generally, cobalt can also react with silicon and leads to the formation of cobalt silicide. Meanwhile, the silicidation reaction with Co participation requires higher temperatures, compared with that by Ni [150]. Nevertheless, it is believed that such conditions can be favorable to lower the number of defects during the graphene formation and to improve the graphene quality [150]. Similarly to the Ni-mediated process, the Co-assisted graphene formation is also very sensitive to changing the technological conditions (such as Co film thickness, annealing time, annealing temperature, cooling rate and heating rate) [151]. For example, it was shown that graphene cannot be formed at the Co film thickness smaller than 50 nm [151]. Overall, this technique allows obtaining of homogeneous coverage of bilayer or monolayer graphene and even its transferring to other substrates [150]. However, Co-assisted graphitization process demands higher temperatures than that of Ni-mediated growth. It is due to the fact the chemical reaction (silicidation) between Co and SiC starts at higher temperatures in comparison to that between Ni and SiC.

A promising approach related to the segregation technique involves using a Ni/Cu catalytic alloy film on 3C-SiC/Si epitaxial films in order to grow high-quality and highly uniform few-layer graphene [153]. It should be mentioned that the choice of the cubic SiC epitaxial layers on Si substrates is caused by the possibilities to avoid undesirable spontaneous polarization-induced doping of graphene (since the spontaneous polarization is zero in the case

of cubic substrate), to lower the fabrication cost (since there is no necessity to use quite expensive bulk SiC substrates for graphitization aims) and to provide a large-area surfaces for graphene growth. Overall, the alloy-assisted graphene formation obeys the same growth mechanism as for the graphene films grown by mediation of Ni catalytic metal. However, the presence of copper changes the graphitization rate. According to the authors' findings, using Ni/Cu alloy is more preferred for graphene growth in comparison to that of Ni alone [153]. It can be explained by the impossibility to provide a homogeneous formation of the nickel silicide over a large SiC surface. This problem causes an irregular distribution of separated islands or even clusters consisting of the nickel silicide phase. In this context, the authors initially suggested and then experimentally demonstrated that utilizing copper in the growth process can provide conditions for more uniform distribution of the Ni atoms over the entire surface of the silicon carbide and can play a role of efficient catalyst to enhance the graphitization rate. Following this technique, this group synthesized high quality and low defect density bilayer graphene uniformly spread over the cubic SiC substrates with quite low Raman I_D/I_G band ratio (~0.2).

Unconventional liquid phase growth of graphene on SiC substrates by mediation of liquid gallium was proposed by H. Hiura et al. [155]. The possibility to growth high-quality graphene layers (with desirable thickness) on different polytypes of SiC was demonstrated. The main point is that liquid gallium plays a dualistic role in the growth process. On one hand, liquid gallium acts as a flux for a temporary storage of carbon. On the other hand, gallium behaves as a catalyst for formation of graphene. The suggested mechanism for gallium-mediated growth is shown in Fig. 17. Overall, this process has two stages. Initially, high temperature heating leads to dissolution of silicon and carbon atoms from SiC into the gallium flux. And then, after cooling to room temperature, carbon atoms precipitate from the flux as graphene. At the same time, the silicon atoms mainly remain in the gallium flux.

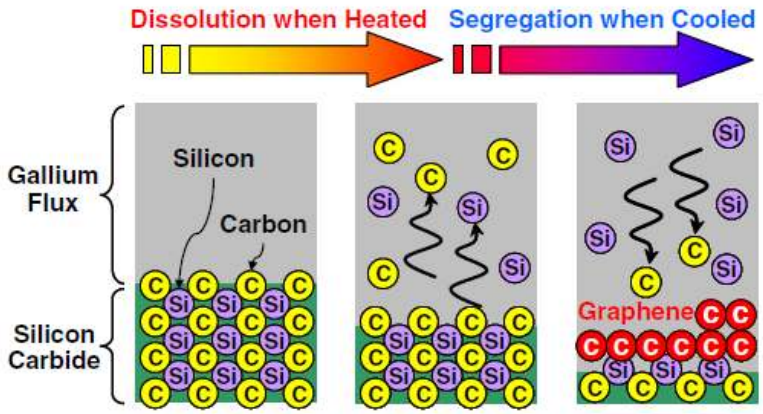

Figure 17. Schematics of the proposed liquid phase growth mechanism. Adapted from H. Hiura et al. [155]. Copyright (2012) Elsevier B.V.

A substrate-free approach to synthesize multilayer graphene on SiC microspheres was implemented by Jun Ma et al. [156]. By a simple template-free pyrolysis of liquid polysilacarbosilane and subsequent annealing in Ar at 1300 °C for 2 h., Ma and co-workers fabricated multi-layer graphene with lateral dimension as large as 100 nm. The growth mechanism is illustrated by Fig. 18. At the initial stage, amorphous SiC microspheres were formed by evaporation and further solidification of the liquid polysilacarbosilane at the temperatures below 900 °C. After this stage, the obtained microspheres were gradually pyrolyzing and shrinking at higher temperatures. At the temperatures reaching 1100°C, the crystallization and phase separation occur. As a result of such transitions, SiC phase and graphite nanocrystal is are formed. Further increase in the temperature up to 1300°C leads to the appearance of an excess carbon, playing a role of additional source for multilayer graphene formation.

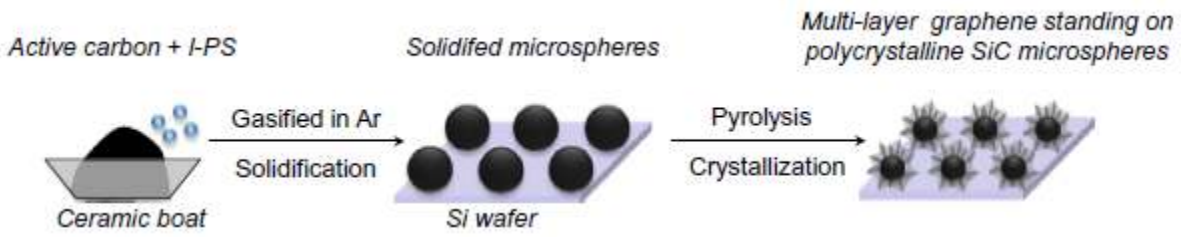

Figure 18. Growth mechanism of multilayer graphene on SiC microspheres. Adapted from Jun Ma et al. [156]. Copyright (2014) Elsevier B.V.

Direct transformation of the SiC nano- and micro-powders with amorphous a-$Si_{1-x}C_x$ nano-shells/films into graphene under low temperatures (800 ºC) and ambient pressure in chlorine (Cl_2) atmosphere was reported by Peng and collaborators [157]. The essence of this approach is that Cl_2 can react with the silicon atoms inside the a-$Si_{1-x}C_x$ nano-shell, thereby forming $SiCl_4$ and thick defective carbon-rich layers (see Figure 19). Immediately after, these defective carbon layers re-organize into thermally stable graphene of few layers (as can be seen in Figure 19). It is important to note that as a result of such process, two different forms of graphene were detected. One of them, i.e epitaxial graphene, is formed only on the surface of the SiC nanoparticles, while the formation features of another observed kind of graphene, wrapped graphene, are not fully understood.

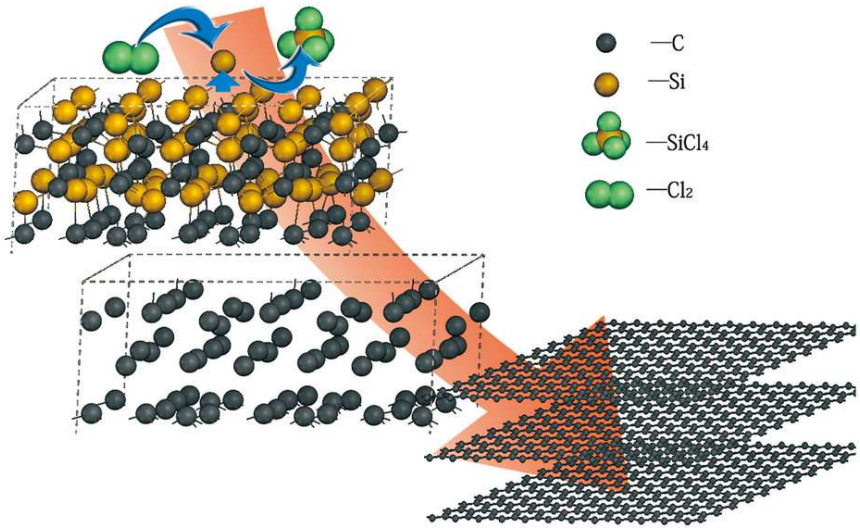

Figure 19. The proposed possible mechanism describing the formation of the graphene layer from amorphous silicon carbide via chlorination. Adapted from Peng et al. [157]. Copyright (2013) Macmillan Publishers Limited.

Summarizing the literature data devoted to attempts to develop the alternative graphene formation techniques on SiC substrates, one needs to emphasize that in spite of some advantages of these approaches (low temperature, low cost) over the traditional ones (thermal decomposition, CVD, MBE), using different mediators (catalytic metals, Cl_2, etc.) complicates the understanding of the physical and chemical nature of the growth mechanisms underlying graphene formation. Therefore, there is no yet consensus concerning what is exactly going on during the self-assembling of carbon atoms in graphene driven by different mediators. Nevertheless, in spite of the debatable growth mechanisms a number of experimental evidences of graphene formation by using such methods exist. Probably the development of alternative methods of graphene synthesis may be important in the light of a strong necessity to reach a trade-off between the fabrication cost and the product quality. We believe that the most promising possible applications of the graphene obtained in such a manner can be for passive elements (conductor, interconnections) in devices and circuits.

3. Summary and concluding remarks

In recent years, the scientific paradigm has shifted from the fundamental “graphene” concept to the search of ways towards realization of hybrid materials and heterostructures with different semiconductors. Such advancements are triggered by the fast progress in (i) synthesis techniques, (ii) deep understanding of “graphene” physics, (iii) improvement of material characterization methodology, and (iv) availability of technologies for high-quality semiconductor materials and device processing. These are prerequisites of a new generation

material development combining the inclusive advantages of well-known semiconductors with more exclusive graphene benefits. To this point, the integration of graphene and SiC is a promising approach towards the benefits of hybrids.

The current literature survey has covered the most important growth mechanisms of epitaxial graphene layers on SiC with consideration of different realistic phenomena, such as presence of step edges, hexagonal pits, silicon vacancies, buffer layer and others. It has been shown that the quality of graphene (number of layers, lateral thickness homogeneity) and its electronic properties are highly sensitive to the status of the SiC substrate including the off-cut angle, different polytypes and face polarity. The main synthesis techniques that are used by the researchers in the field are thermal decomposition (sublimation) of SiC (the latter being also a substrate), CVD and MBE. The latter two methods utilize external carbon sources and the graphene synthesis proceeds in a bottom up mode, while SiC sublimation is a self-organized graphene synthesis in a top down manner. Both sublimation growth and CVD are rather high temperature methods (T>1200C) but this is an advantage when aiming at high structural quality graphene. Concomitantly, when approaching graphene by SiC surface graphitization, the first rate modified surface (reconstruction) cannot be fully decoupled from the substrate but the so-called 0-layers graphene or buffer layer is formed, especially on the Si terminated face (0001). To date the role of this layer is well understood and it is two-fold: degrading electrical properties due to additional doping and carrier scattering while enabling high structural quality on a large area due to epitaxial growth conditions. In fact, graphene can be made buffer free or quasi free standing by using intercalation.

Alternative methods have been proposed, mainly based on carbon segregation via metal silicide formation with the SiC substrate at moderate temperatures. The graphene obtained is not of exceptional quality but can be used for passive elements (conductors) in devices and circuits.

To conclude, combining graphene with SiC can be realized by different techniques. The most advanced is the one based on thermal decomposition of SiC. In addition to the good process understanding and ability to control, this technique is environment-friendly and safe. CVD of graphene on SiC has been not so popular but it is promising especially for production scale although safety issues may be of concern. While MBE is still a fundamentally oriented technique with a high potential for novel heterostructures mediated by graphene.

4. Acknowledgements

The authors would like to thank the Graphene Flagship EU project GrapheneCore 1 (Grant 696656, VR grant 621-2014-5805, KAW foundation and Ångpanneföreningens Forskningsstiftelse (Grant 14-517; Grant 16-541). V. Khranovskyy acknowledges the support

from Swedish Research Council (VR) Marie Skłodowska Curie International Career Grant #2015-00679 ”GREEN 2D FOX”.

5. References

[1] Putz M V and Ori O 2015 *Exotic Properties of Carbon Nanomatter* (New York: Springer)

[2] Kroto H W, Heath J R, O’Brien S C, Curl R F, Smalley R E 1985 *Nature* **318** 162

[3] Iijima S 1991 *Nature* **354** 56

[4] Krainyukova N, Zubarev E 2016 *Phys. Rev. Lett.* **116** 055501

[5] Boehm H P, Clauss A, Fischer G O and Hofmann U 1962 *Z. anorg. allg. Chem*. **316** 119

[6] Landau L D 1937 *Phys. Z. Sowjetunion* **11** 26

[7] Mermin N D 1968 *Phys. Rev.* **176** 250

[8] Wallace P R 1947 *Phys. Rev.* **71** 622

[9] Slonczewski J C and Weiss P R 1958 *Phys. Rev.* **109** 272

[10] Novoselov K S, Geim A K, Morozov S V, Jiang D, Zhang Y, Dubonos S V, Grigorieva I V, Firsov A A 2004 *Science* **306** 666

[11] Morgan A E, Somarjai G A 1968 *Surf. Sci.* **12** 405

[12] May J W 1969 *Surf. Sci.* **17** 267

[13] Shelton J C, Patil H R, Blakely J M 1974 *Surf. Sci.* **43** 493

[14] Van Bommel A J, Crombeen J E, Van Tooren A 1975 *Surf. Sci.* **48** 463

[15] Berger C, Song Z, Li T, Li X, Ogbazghi A Y, Feng R, Dai Z, Marchenkov A N, Conrad E H, First P N, de Heer W A 2004 *J.Phys. Chem. B* **108** 19912

[16] Bunch J S *et al* 2007 *Science* **315** 490

[17] Balandin A A, Ghosh S *et al* 2008 *Nano Lett.* **8** 902

[18] Ghosh S, Calizo I *et al* 2008 *Appl. Phys. Lett.* **92** 151911

[19] Novosevov K S *et al* 2007 *Phys. Stat. Sol. (b)* **244** 4106

[20] Katsnelson M I *et al.* 2006 *Nature Physics* **2** 620

[21] Tzalenchuk A, Lara-Avila S, Kalaboukhov A, Paolillo S, Syvajarvi M, Yakimova R, Kazakova O, Janssen T J B M, Fal’ko V, Kubatkin S 2010 *Nat. Nanotechnol.* **5** 186

[22] Javier García de Abajo F 2014 *ACS Photonics* **1** 135

[23] Geim A K and Novoselov K S 2007 *Nature Mat.* **6** 183

[24] Novoselov K S *et al* 2005 *PNAS* **102** 10451

[25] Bolotin K I *et al* 2008 *Phys. Rev. Lett*. **101** 096802

[26] Niyogi S, Bekyarova E, Itkis M E, McWilliams J L, Hamon M A and Haddon R C 2006 *J. Am. Chem. Soc.* **128** 7720

[27] Zhang Y *et al* 2013 *Acc. Chem. Res.* **46** 2329

[28] Muñoz R and Gómez-Aleixandre C 2013 *Chem. Vap. Deposition* **19** 297

[29] Tetlow H *et al* 2014 *Phys. Rep.* **542** 195

[30] Yi M, Shen Z 2015 *J. Mater. Chem.* A **3** 11700

[31] Riedl C *et al* 2010 *Journal of Physics D: Applied Physics* **43** 374009

[32] Wu P *et al* 2014 *Small* **10** 2136

[33] Norimatsu V, Kusunoki M 2014 *Semicond. Sci. Technol.* **29** 064009

[34] Norimatsu V, Takada J, Kusunoki M 2011 *Phys. Rev. B* **84** 035424

[35] Emtsev *et al* 2008 *Phys. Rev. B* **77** 155303

[36] Robinson Z R *et al* 2015 *Carbon* **81** 73

[37] Giusca C E, Spencer S J, Shard A G, Yakimova R, Kazakova O 2014 *Carbon* **69** 221

[38] Tejeda A, Taleb-Ibrahimi A, De Heer W, Berger C, Conrad E H 2012 *New J. Phys.***14** 125007

[39] Sprinkle M, Hicks J, Tejeda A, Taleb-Ibrahimi A, Le Fevre P, Bertran F, Tinkey H, Clark M C, Soukiassian P, Martinotti D, Hass J and Conrad E H 2010 *J. Phys. D: Appl. Phys.* **43** 374006

[40] Geim A. K, Grigorieva I V 2013 *Nature* **499** 419

[41] Tromp R, Hannon J B 2009 *Phys. Rev. Lett.* **102** 106104

[42] Syväjärvi M, Yakimova R, Janzén E 1999 *J. Electrochem. Soc.* **146** 1565

[43] Dharmaraj P *et al* 2013 *J. Phys. Chem. C* **117** 19195

[44] Hannon J B, Copel M, Tromp R M. 2011 *Phys. Rev. Lett.* **107** 166101

[45] Ostler M, Koch R J, Speck F, Fromm F, Vita H, Hundhausen M, Horn K, Seyller T 2012 *Mater. Sci. Forum* **717** 649

[46] Kowalski G, Tokarczyk M, Dąbrowski P, Ciepielewski P, Możdżonek M, Strupiński W and Baranowski J M 2015 *J. Appl. Phys.* **117** 105301

[47] Watcharinyanon S, Virojanadara C, Osiecki J, Zakharov A A, Yakimova R, Uhrberg R and Johansson L I 2011 *Surf. Sci.* **17-18** 1662

[48] Xia C, Watcharinyanon S, Zakharov A A, Yakimova R, Hultman L, Johansson L I and Virojanadara C 2012 *Phys. Rev. B* **85** 045418

[49] Emtsev K V, Zakharov A A, Coletti C, Forti S and Starke U 2011 *Phys. Rev. B* **84** 125423

[50] Ostler M, Fromm F, Koch R J, Wehrfritz P, Speck F, Vita H *et al* 2014 *Carbon* **70** 258

[51] Wong S L, Khoo K H, Quek S Y and Wee A T S 2015 *J. Phys. Chem. C* **119** 29193

[52] Xia C, Johansson L I, Zakharov A A, Hultman L and Virojanadara C 2014 *Mater. Res. Express* **1** 1

[53] Bisti F, Profeta G, Vita H, Donarelli M, Perrozzi F, Sheverdyaeva P M, Moras P, Horn K, and Ottaviano L 2015 *Phys. Rev. B* **91** 245411

[54] Xia C, Johansson L I, Niu Y, Zakharov A A, Janzén E, Virojanadara C 2014 *Carbon* **79** 631

[55] Gierz I, Suzuki T, Weitz R T, Lee D Su, Krauss B, Riedl C, Starke U, Höchst H, Smet J H, Ast C R, and Kern K 2010 *Phys. Rev. B* **81** 235408

[56] Xia C, Watcharinyanon S, Zakharov A A, Johansson L I, Yakimova R, Virojanadara C 2013 *Surf. Sci.* **613** 88

[57] Watcharinyanon S, Johansson L I, Xia C, Flege J I, Meyer A, Falta J, Virojanadara C 2013 *Graphene* **2** 66

[58] Sung S J, Yang J W, Lee P R, Kim J G, Ryu M T, Park H M, Lee G, Hwang C C, Kim K S, Kim J S, Chung J W 2014 *Nanoscale* **7** 3824

[59] Li K, Feng X, Zhang W, Ou Y, Chen L, He K, Wang L L, Guo L, Liu G, Xue Q K and Ma X 2013 *Appl. Phys. Lett.* **103** 062601

[60] Petrović M, Šrut Rakić I, Runte S, Busse C, Sadowski J T, Lazić P, Pletikosić I, Pan Z H, Milun M, Pervan P, Atodiresei N, Brako R, Šokčević D, Valla T, Michely T & Kralj M 2013 *Nat. Commun.* **4** 2772

[61] Yagyu K, Tajiri T, Kohno A, Takahashi K, Tochihara H, Tomokage H and Suzuki T 2014 *Appl. Phys. Lett.* **104** 05311

[62] Mattausch A, Pankratov O 2007 *Phys. Rev. Lett.* **99** 076802

[63] Varchon F *et al* 2007 *Phys. Rev. Lett.* **99** 126805

[64] Al-Temimy A, Riedl C, Starke U 2009 *Appl. Phys. Lett.* **95** 231907

[65] Luxmi et al 2010 *Phys. Rev. B* **82** 235406

[66] Jernigan G G et al 2009 *Nano Lett.* **9** 2605

[67] Daas B K et al 2012 *Cryst. Growth Des.* **12** 3379

[68] Ni Z H et al 2008 *Phys. Rev. B.* **77** 115416

[69] Shetu S S et al 2013 *J. Appl. Phys.* **114** 164903

[70] Darakchieva V *et al* 2013 *Appl. Phys. Lett.* **102** 213116

[71] Kim M *et al* 2012 *Nanotechnol.* **23** 335202.

[72] Badami D V 1962 *Nature* **193** 569

[73] Kageshima H, Hibino H, Yamaguchi H, Nagase M 2011 *Jpn. J. Appl. Phys.* **50** 095601

[74] Ohta T, Bartelt N C, Nie S, Thürmer K and Kellogg G L 2010 *Phys. Rev. B* **81** 121411R

[75] Varchon F, Mallet P, Veuillen J Y and Magaud L 2008 *Phys. Rev. B* **77** 235412

[76] Tapaszto L *et al* 2012 *Nat. Phys.* **8** 739

[77] Matsui H, Matsui F, Maejima N, Matsushita T, Daimon H 2015 *Surf. Sci.* **635** 1

[78] Ouerghi A, Ridene M, Mathieu C, Gogneau N and Belkhou R 2013 *Appl. Phys. Lett.* **102** 253108

[79] Ming F and Zangwill A 2011 *Phys. Rev. B* **84** 115459

[80] Poon S W, Chen W, Wee A T S and E S Tok 2010 *Phys. Chem. Chem. Phys.* **12** 13522

[81] Tang C, Meng L, Xiao H and Zhong J 2008 *J. Appl. Phys.* **103** 63505

[82] Virojanadara C, Syvajarvi M, Yakimova R, Johansson L, Zakharov A, Balasubramanian T 2008 *Phys. Rev. B* **78** 1

[83] Yager T, Lartsev A, Yakimova R, Lara-Avila S, Kubatkin S 2015 *Carbon* **87** 409

[84] Virojanadara C, Yakimova R, Osiecki J R, Syvajarvi M, Uhrberg R I G, Johansson L I *et al* 2009 *Surf. Sci.* **603** L87

[85] Huang H, Chen W, Chen S, Wee A 2008 *ACS Nano* **2** 2513

[86] Wang D, Liu L, Chen W, Chen X, Huang H, He J, Feng Y P, Wee A T S and Shen D 2015 *Nanoscale* **14** 4522

[87] Zhang R, Li H, Zhang Z D, Wang Z S, Zhou S Y, Wang Z, Li T C, Liu J R, Fu D J 2015 *Nucl. Instrum. Methods Phys. Res., Sect. B* **356–357** 99

[88] Strupinski W, Grodecki K, Caban P, Ciepielewski P, Jozwik-Biala I, Baranowski J M 2015 *Carbon* **81** 63

[89] Park J H, Mitchel W C, Grazulis L, Eyink K, Smith H E, Hoelscher J E 2011 *Carbon* **49** 631

[90] Hannon J B, Tromp R M 2008 *Phys. Rev. B* **77** 241404R

[91] Kageshima H, Hibino H, Yamaguchi H, and Nagase M 2013 *Phys. Rev. B* **88** 235405

[92] Norimatsu W, Kusunoki M 2010 *Physica E* **42** 691

[93] Osaklung J *et al* 2012 *Appl. Surf. Sci.* **258** 4672

[94] Ruammaitree A, Nakahara H, Saito Y 2014 *Appl. Surf. Sci.* **307** 136

[95] Hattori A N, Okamoto T, Sadakuni S, Murata J, Arima K, Sano Y, Hattori K, Daimon H, Endo K, Yamauchi K 2011 *Surf. Sci.* **605** 597

[96] Camara N *et al* 2010 *Appl. Phys. Lett.* **97** 093107

[97] Eddy C R, Gaskill D K 2009 *Science* **324** 1398

[98] Giannazzo F *et al* 2014 *J. Cryst. Growth* **393** 150

[99] Kajiwara T *et al* 2013 *Phys. Rev. B* **87** 121407(R)

[100] Penuelas J *et al* 2009 *Phys. Rev. B* **79** 033408

[101] Kisoda K *et al* 2010 *Appl. Phys. Lett.* **97** 033108

[102] Tanaka S *et al* 2010 *Phys. Rev. B* **81** 041406R

[103] Ji S H *et al* 2012 *Nat. Mater.* **11** 114

[104] Nakatsuji K *et al* 2012 *Phys. Rev. B* **85** 195416; Nakatsuji K *et al* 2010 *Phys. Rev. B* **82** 045428

[105] Hupalo M, Conrad E H, Tringides M C 2009 *Phys. Rev. B* **80** 041401(R)

[106] Dimitrakopoulos C *et al* 2011 *Appl. Phys. Lett.* **98** 222105

[107] Robinson J A *et al* 2011 *Appl. Phys. Lett.* **98** 222109

[108] Nelson F *et al* 2012 *J. Vac. Sci. Technol., B* **30** 04E106

[109] Ostler M, Deretzis I, Mammadov S, Giannazzo F, Nicotra G, Spinella C *et al* 2013 *Phys. Rev. B* **88** 085408

[110] Hens P *et al* 2014 *Carbon* **80** 823

[111] Xu P *et al* 2014 *Carbon* **80** 75

[112]Xu P *et al* 2013 *Surf. Sci.* **617** 113

[113] Lin J *et al* 2014 *Appl. Phys. Lett.* **104** 183102

[114] Michon A *et al* 2010 *Appl. Phys. Lett.* **97** 171909

[115] Yakimova R *et al* 2014 *Physica B* **439** 54

[116] Yazdi G R *et al* 2013 *Carbon* **57** 477

[117] Boosalis A *et al* 2012 *Appl. Phys. Lett.* **101** 011912

[118] Coletti C *et al* 2013 *Phys. Rev. B* **88** 155439

[119] Hwang C, Siegel D A, Mo S K, Regan W, Ismach A, Zhang Y, Zettl A and Lanzara A 2012 *Sci. Rep.* **2** 590

[120]Sławinska J *et al* 2015 *Carbon* **93** 88

[121] Ciuk T *et al* 2015 *Carbon* **93** 1042

[122] Mammadov S, Ristein J, Koch R J, Ostler M, Raidel C, Wanke M, Vasiliauskas R, Yakimova R and Seyller T 2014 *2D Materials* **1** 035003

[123] Grodecki K, Blaszczyk J A, Strupinski W, Wysmolek A, Stępniewski R, Drabinska A, Sochacki M, Dominiak A, and Baranowski J M 2012 *J. Appl. Phys.* **111** 114307

[124] Wierzbowska M, Dominiak A, Tokar K 2013 *Phys.Chem. Chem. Phys.* **15** 8805

[125] Cai S, Liu Z, Zhong N, Liu S, Liu X 2015 *Materials* **8** 5586-5596

[126] Michon A, Vezian S, Roudon E, Lefebvre D, Zielinski M, Chassagne T, and Portail M 2013 *J. Appl. Phys.* **113** 203501

[127] Kim J G, Kim W S, Kim Y H, Lim C H , Choi D J 2013 *Surf. Coat. Technol.* **231** 189.

[128] Strupinski W, Grodecki K, Wysmolek A, Stepniewski R, Szkopek T, Gaskell P E, Gruneis A, Haberer D, Bozek R, Krupka J, Baranowski J M 2011 *Nano Lett.* **11** 1786

[129] Michon A, Largeau L, Mauguin O, Ouerghi A, Vézian S, Lefebvre D, Roudon E, Zielinski M, Chassagne T, Portail M 2012 *Phys. Status Solidi C* **9** 175–178

[130] Urban J M, Dąbrowski P, Binder J, Kopciuszyński M, Wysmołek A, Klusek Z, Jałochowski M, Strupiński W, Baranowski J M 2014 *J. Appl. Phys*.**115** 233504

[131] Lafont F, Ribeiro-Palau R, Kazazis D, Michon A, Couturaud O, Consejo C, Chassagne T, Zielinski M, Portail M, Jouault B, Schopfer F, Poirier W 2015 *Nat. Commun.* **6** 6806

[132] Jabakhanji B, Michon A, Consejo C, Desrat W, Portail M, Tiberj A, Paillet M, Zahab A, Cheynis F, Lafont F, Schopfer F, Poirier W, Bertran F, Le F`evre P, Taleb-Ibrahimi A, Kazazis D, Escoffier W, Camargo B C, Kopelevich Y, Camassel J, Jouault B 2014 *Phys. Rev. B* **89** 085422

[133] Gajewski K, Kopiec D, Moczała M, Piotrowicz A, Zielony M, Wielgoszewski G, Gotszalk T, Strupinski W 2015 *Micron* **68** 17

[134] Portail M, Michon A, Ve´zian S, Lefebvre D, Chenot S, Roudon E, Zielinski M, Chassagne T, Tiberj A, Camassel J, Cordie Y 2012 *J. Crystal Growth* **349** 27

[135] Hwang J, Shields V B, Thomas C I, Shivaraman S, Hao D, Ki M, Woll A R, Tompa G S, Spencer M G 2010 *J. Crystal Growth* **312** 3219

[136] Tokarczyk M, Kowalski G, Możdżonek M, Borysiuk J, Stępniewski R, Strupiński W, Ciepielewski P, Baranowski J M 2013 *Appl. Phys. Lett.* **103** 241915

[137] Grodecki K, Bozek R, Strupinski W, Wysmolek A, Stepniewski R, Baranowski J M 2012 *Appl. Phys. Lett.* **100** 261604

[138] Moreau E, Godey S, Ferrer F J, Vignaud D, Wallart X, Avila J, Asensio M C, Bournel F, Gallet J J 2010 *Appl. Phys. Lett.* **97** 241907

[139] Moreau E, Ferrer F J, Vignaud D, Godey S, Wallart X 2010 *Phys. Status Solidi A* **207** 300

[140] Moreau E, Godey S, Wallart X, Razado-Colambo I, Avila J, Asensio M C, Vignaud D 2013 *Phys. Rev. B* **88** 075406

[141] Razado-Colambo I, Avila J, Chen C, Nys J P, Wallart X, Asensio M C, Vignaud D 2015 *Phys. Rev. B* **92** 035105

[142] Juang Z Y, Wu C Y, Lo C W, Chen W Y, Juany C F, Hwang J C, Chen F R, Leou K C, Tsai C H 2009 *Carbon* **47** 2026

[143] Woodworth A A, Stinespring C D 2010 *Carbon* **48** 1999

[144] Vassilevski K, Nikitina I P, Horsfall A B, Wright N G, Johnson C M 2010 *Mater. Sci. Forum* **645** 589.

[145] Yoneda T, Shibuya M, Mitsuhara K, Visikovskiy A, Hoshino Y, Kido Y 2010 *Surf. Sci.* **604** 1509

[146] Macháč P, Fidler T, Cichoň S, Mišková L 2012 *Thin Solid Films* **520** 5215

[147] Kang C Y, Fan L L, Chen S, Liu Z L, Xu P S, Zou C W 2012 *Appl. Phys. Lett.* **100** 251604

[148] Li D, Zeng X, Yang Y, Yang J, Yuan W 2012 *Mater. Lett.* **74** 19

[149] Escobedo-Cousin E, Vassilevski K, Hopf T, Wright N, O'Neill A, Horsfall A, Goss J, Cumpson P 2013 *J. Appl. Phys.* **113** 114309

[150] Li C, Li D, Yang J, Zeng X, Yuan W 2011 *J. Nanomater.* **2011** 319624.

[151] Machac P, Fidler T, Cichon S, Jurka V 2013 *J. Mater. Sci.: Mater. Electron.* **24** 3793

[152] Cichoň S, Mišková L, Vondráček M 2014 *Appl. Surf. Sci.* **320** 544

[153] Iacopi F, Mishra N, Cunning B V, Goding D, Dimitrijev S, Brock R, Dauskardt R H, Wood B, Boeckl J 2015 *J. Mater. Res.* **30** 609

[154] Lee M V, Hiura H, Tyurnina AV, Tsukagoshi K 2012 *Diamond Relat. Mater.* **24** 34.

[155] Hiura H, Lee M V, Tyurnina A V, Tsukagoshi K 2012 *Carbon* **50** 5076

[156] Ma J, Li G, Chu Z, Li X, Li Y, Hu T 2014 *Carbon* **69** 634

[157] Peng T, Lv H, He D, Pan M & Mu S 2013 *Sci. Rep.* **3** 1148